On predicting heterogeneity in nanoparticle dosage

Celia V. Dowling

School of Mathematics and Statistics, The University of Melbourne, Australia.

Paula M. Cevaal

Department of Microbiology and Immunology, The University of Melbourne at the Peter Doherty Institute for Infection and Immunity, Australia.

Matthew Faria

Department of Biomedical Engineering, The University of Melbourne, Australia.

Stuart T. Johnston*

School of Mathematics and Statistics, The University of Melbourne, Australia.

Abstract

Nanoparticles are increasingly employed as a vehicle for the targeted delivery of therapeutics to specific cell types. However, much remains to be discovered about the fundamental biology that dictates the interactions between nanoparticles and cells. Accordingly, few nanoparticle-based targeted therapeutics have succeeded in clinical trials. One element that hinders our understanding of nanoparticle-cell interactions is the presence of heterogeneity in nanoparticle dosage data obtained from standard experiments. It is difficult to distinguish between heterogeneity that arises from stochasticity in nanoparticle behaviour, and that which arises from heterogeneity in the cell population. Mathematical investigations have revealed that both sources of heterogeneity contribute meaningfully to the heterogeneity in nanoparticle dosage. However, these investigations have relied on simplified models of nanoparticle internalisation. Here we present a stochastic mathematical model of nanoparticle internalisation that incorporates hitherto neglected biological phenomena such as multistage internalisation, cell division, asymmetric nanoparticle inheritance and nanoparticle saturation. Critically, our model provides information about nanoparticle dosage at an individual cell level. We perform model simulations to examine the influence of specific biological phenomena on the heterogeneity in nanoparticle dosage. Under certain modelling assumptions, we derive analytic approximations of the nanoparticle dosage distribution. We demonstrate that the analytic approximations are accurate, and show that nanoparticle dosage can be described by a Poisson mixture distribution with rate parameters that are a function of Beta-distributed random variables. We discuss the implications of the analytic results with respect to parameter estimation and model identifiability from standard experimental data. Finally, we highlight extensions and directions for future research.

Keywords: Nanoparticles, stochastic modelling, heterogeneity, dosage distribution, cell division, nanoparticle-cell interactions.
2010 MSC: 92B05

*Corresponding author
Email address: stuart.johnston@unimelb.edu.au (Stuart T. Johnston)

1. Introduction

Nanoparticle-based therapeutics are at the forefront of precision medicine, as nanoparticles are able to deliver payloads to specific locations in the body [1, 2]. This technology has seen widespread usage in mRNA vaccines for COVID-19, where lipid nanoparticles coated by polyethylene glycol are used to encapsulate mRNA and deliver it to the immune system [1]. Nanoparticles have significant potential beyond vaccine delivery, such as for the treatment of malignant tumours [3]. If nanoparticles that carry chemotherapeutics interact preferentially with the tumour cell population, the tumour can be effectively treated while the toxic side effects of chemotherapy are ameliorated [3]. However, we do not currently understand how the physicochemical properties of a nanoparticle inform its ability to preferentially interact with a specific cell population [2, 3, 4]. Further, we cannot predict the *in vivo* behaviour of nanoparticles in humans from *in vitro* experiments or animal models [2]. As such, few clinical trials of nanoparticle-based therapeutics have succeeded [5]. Significant work remains to achieve a more complete understanding of nanoparticle-cell interactions and improve the development pipeline of nanoparticle-based therapeutics.

One factor that hinders understanding of the interactions between nanoparticles and cells is heterogeneous experimental data [6, 7, 8, 9, 10]. In standard experiments there is heterogeneity in the number of nanoparticles internalised across a cell population, even though experiments are conducted on clonally-identical cell lines [6, 7, 8, 9, 10]. We will refer to heterogeneity in the number of internalised particles as the *dosage distribution*. The presence of a dosage distribution has implications about the effective treatment of the entire cell population [11]. As with all therapies, there is a threshold dose that must be internalised by an individual cell for that cell to be considered "treated," known as the therapeutic dose [12]. It is therefore critical to understand whether any heterogeneity in experimental data arises from heterogeneity in the underlying biology of the cell population, or whether the heterogeneity can be attributed to the stochastic nature of nanoparticle motion [6, 7, 8, 9, 10]. If the dosage distribution arises from differences in cell characteristics, a certain portion of the cell population may not receive a therapeutic dose of nanoparticles [6]. Treatment-resistant cell subpopulations, even if rare, can be a critical factor in determining whether a disease progresses or is cured [13, 14].

Mathematical models are a natural tool to unravel the origins of heterogeneity in experimental data [6, 7, 9]. Previous investigations have highlighted how heterogeneous data from *in vitro* experiments arises from a combination of the stochastic nature of nanoparticle motion and the biological heterogeneity inherent to cell populations [6, 7]. However, these investigations have relied on simplified descriptions of the interactions between nanoparticles and cells. For example, previous studies[6, 7] have considered a single stage association model of nanoparticle-cell interactions, where nanoparticles become irreversibly associated to cells. Note that *association* refers to nanoparticles that are either *bound* to the cell membrane or are *internalised* by the cell [15, 16]. Common high-throughput experimental methods cannot distinguish between these two states [15]. In this simplified model, the dosage distribution resulting from stochastic nanoparticle motion is shown to be Poisson distributed with a rate parameter that corresponds to the rate that nanoparticles arrive at the cells [6, 7]. This result relies on several simplifying assumptions, such as an absence of both cell proliferation and rate-limited internalisation processes. However, in reality, the process by which nanoparticles are internalised is significantly more complicated, and involves multiple steps that can include nanoparticle-membrane binding, cell receptor recruitment, nanoparticle-receptor binding, membrane deformation, and nanoparticle recycling [4, 17]. Models that include some or all of these steps have been presented previously in a deterministic context (see the review of Johnston *et al.* [18] and references therein, for example). However, these models have not been presented in a stochastic context and hence do not provide insight about the interplay between specific internalisation processes and unavoidable heterogeneity in dosage. Note that stochasticity refers to randomness in the amount of time required for a particular component of the nanoparticle internalisation process, such as nanoparticle-receptor binding or membrane deformation, to occur. This definition is consistent with previous investigations into the source of heterogeneity in

nanoparticle dosage distributions [6, 7]. Studies have demonstrated that the simplifying assumptions made in investigations of heterogeneous dosage distributions are not always appropriate [19, 20]. For example, it has been observed that nanoparticle association is a saturating process, where only a finite number of nanoparticles are able to associate to an individual cell [19]. This implies that the rate of nanoparticle association decreases with the number of previously-associated nanoparticles, and hence the dosage distribution is no longer Poisson [6]. Similarly, the inheritance of nanoparticles during cell division is an asymmetric process [8, 20, 21]. Therefore, if any cell division occurs during the course of an experiment, the assumption of a Poisson dosage distribution is no longer appropriate. Additionally, it is currently unclear how the different components of the nanoparticle internalisation process influence the dosage distribution. Consequently, it is not straightforward to predict how much heterogeneity will be present in measured nanoparticle dosage distributions, even in the absence of any confounding measurement noise or heterogeneity in the underlying cell population. If we cannot tell how much of the heterogeneity in dosage is unavoidable in the best case scenario, we cannot determine how much of the heterogeneity in dosage can be attributed to heterogeneity in cell characteristics.

Here we present an agent-based model of nanoparticle-cell interactions that provides information about the number of nanoparticles in each phase of the internalisation process at an individual cell level. The model includes relevant cell behaviour, such as the ability for cells to move and to undergo division via cell cycle progression. We examine the nanoparticle dosage distribution that arises in a range of scenarios, including where multistage internalisation, rate-limited internalisation, and cell division are relevant. We demonstrate that the previous assumption that dosage distributions that arise from stochasticity in nanoparticle internalisation are Poisson distributed is not always appropriate. We present analytic expressions for the expected dosage distributions and the amount of heterogeneity in certain simplified cases. In each case, we verify that the analytic expression describes the behaviour in the agent-based model. Crucially, our work provides a method for predicting the expected heterogeneity in nanoparticle dosage arising from stochastic internalisation processes. This is distinct from the heterogeneity in dosage that arises from heterogeneity in the characteristics of the underlying cell population. By comparing the predicted dosage distribution with the heterogeneity present in experimental data, we can isolate and observe any heterogeneity in the underlying cell biology. Based on the analytic results, we discuss heuristic methods for conducting parameter estimation on experimental data. We highlight the importance of measuring certain experimental quantities to be able to estimate key biological parameters, and to be able to distinguish between biological mechanisms that have a similar influence on nanoparticle internalisation. Finally, we discuss avenues and extensions for future research.

2. Methods

A standard experimental approach to examine the therapeutic potential of a novel nanoparticle is a nanoparticle-cell association assay, a schematic of which is presented in Figure 1. [16, 22]. In an association assay, a cell population is seeded in a culture dish and allowed to grow for a specified amount of time [22]. In certain cases, this time may be sufficient for the cell population to reach confluence. However, this is not always not the case [23], particularly if the cell line of interest has a long doubling time. Here we focus on association assays for adherent cell lines, where the cells grow on the bottom of the culture dish, though we note that experiments are also performed for suspension cell lines, where the cells are suspended in culture media. The experiment effectively begins when the cell culture media is replaced with fresh media that contains a suspension of nanoparticles. During the course of the experiment, the nanoparticles move through the fluid and interact with the cells at the bottom of the culture dish [19, 24]. Nanoparticle motion is driven by a combination of sedimentation and diffusion, which represents gravity-driven and random motion, respectively [19, 24, 25, 26]. The effects of sedimentation can be ameliorated by either continuously mixing the culture media, or by selecting small and/or light nanoparticles [27]. Nanoparticles interact with cells via a range of biological mechanisms, including receptor and surface binding, and can become internalised through a number

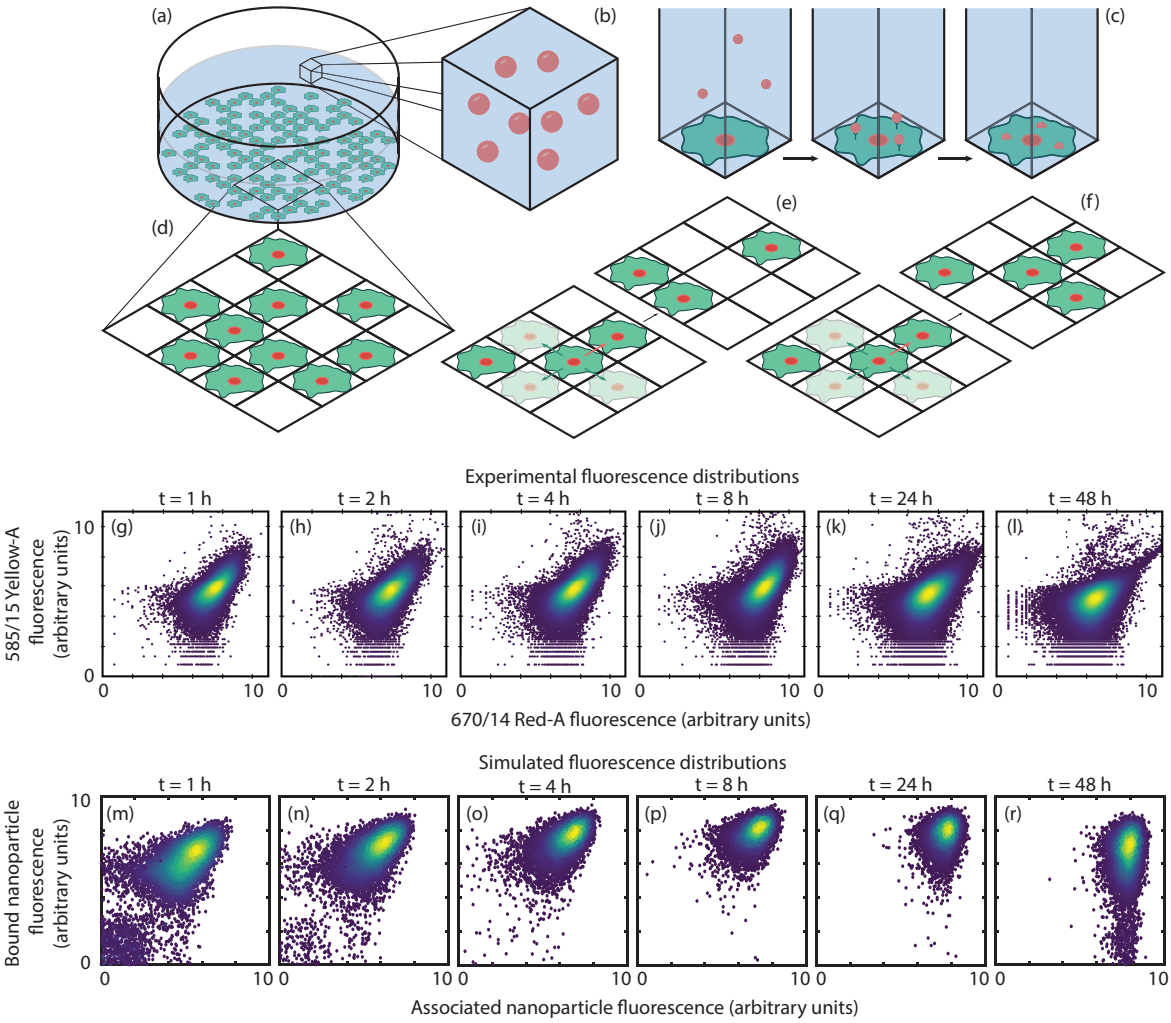

Figure 1: Schematic of standard nanoparticle-cell experiments and the modelling framework. (a) Cells are seeded on a culture dish and (b) immersed in a fluid containing a nanoparticle suspension. (c) Nanoparticles undergo transport through the fluid, bind to the cells, and ultimately become internalised. (d) Cell behaviour on the culture dish is represented via a lattice-based random walk. (e) Example motility events on the lattice, where the cell attempts to move to one of four nearest-neighbour sites. (f) Example proliferation events on the lattice, where the cell attempts to place a daughter cell on one of four nearest-neighbour sites. Green arrows indicate events that will be successful while red arrows indicate events that will not be successful. (g)-(l) Experimental fluorescence distributions for 100 nm protein G coated iron oxide nanoparticles and Jurkat T cells measured after 1, 2, 4, 8, 24 and 48 hours. High density regions are shown in yellow, low density regions are shown in blue. The captured fluorescence signals correspond to membrane-bound nanoparticles (585/15 Yellow-A) and associated nanoparticles (670/14 Red-A). (m)-(r) Representative fluorescence distributions with added measurement noise obtained from the simulation after 1, 2, 4, 8, 24 and 48 hours. Membrane-bound nanoparticle dosage and associated nanoparticle dosage are presented in arbitrary units. Experimental details are presented in Appendix A.

of endocytic pathways [4, 17]. Typically in an association assay, the number of nanoparticles that are either strongly bound to the cell surface or have been internalised by the cell are recorded [15, 19]. It is not straightforward to distinguish between strongly-bound and internalised nanoparticles [15]. Therefore, the output of an association assay is usually the average number of nanoparticles associated per cell reported at a small number of time points [22]. Through the use of appropriate mathematical models, parameters that represent the rate of interaction between nanoparticles and cells can be estimated from such data [19].

Here we develop and introduce a stochastic mathematical model of a nanoparticle-cell association assay. Our modelling framework has two components: a lattice-based random walk for the cell population and a multistage stochastic model of nanoparticle internalisation (Figure 1). Crucially, our modelling framework provides detail at the level of individual cells. This allows for direct comparison of the model output with association assay data (Figures 1(g)-(r)), both where only association data is available, and where more sophisticated techniques have been employed and hence bound and internalised nanoparticles can be distinguished. A widespread approach is to use flow cytometry to measure the number of associated nanoparticles [15, 19, 22]. Flow cytometry provides information about $\sim 10^5$ individual cells at each time point in an experiment. Further, the modelling framework captures the stochasticity of nanoparticle internalisation, which is driven by the inherent random motion of the nanoparticles and the stochastic duration of binding and internalisation events [6]. This allows for the delineation of heterogeneity in dosage that arises from inherently stochastic internalisation processes, and heterogeneity in dosage that arises from heterogeneity in cell characteristics.

2.1. Cell population model

To describe the behaviour of the adherent cell population, we consider a lattice-based random walk on a two-dimensional square lattice of size $X\Delta$ by $Y\Delta$ where Δ is the lattice width [28] (Figure 1(d)). The random walk is chosen to be an exclusion process, where each lattice site may be occupied by, at most, one agent [28, 29]. Here agents represent cells and Δ is chosen to be equivalent to a cell diameter. We impose periodic boundary conditions on the lattice. That is, an agent that leaves the domain is immediately replaced by an identical agent on the opposite side of the domain [30]. The simulation domain can therefore be considered as a representative subsection of a larger experimental domain [30]. It is typically computationally infeasible to simulate the entire experimental domain due to the large number of cells present [30].

Agents on the lattice undergo motility and proliferation events [31]. We make the assumption that cell death does not play a significant role in the experiment, that is, that the nanoparticle dose is not cytotoxic. For a motility event, an agent is randomly selected, with replacement, with probability M during a timestep of duration τ. The agent, located at $(x\Delta, y\Delta)$, attempts to move to a target site that is randomly selected from the four nearest-neighbour sites located at $(x\Delta \pm \Delta, y\Delta)$ and $(x\Delta, y\Delta \pm \Delta)$. The motility event will be successful if the target site is unoccupied, and will otherwise be aborted (Figure 1(e)) [28, 29, 30, 31].

To represent cell division, we consider a multistage proliferation process [32]. Including multiple stages, denoted $1 \leq p \leq \Pi$, in the proliferation process allows for cell cycle behaviour to be incorporated in the model. The cell cycle is typically considered as four distinct stages: Gap 1 (G1), Synthesis (S), Gap 2 (G2), and Mitosis (M), with cell division occurring at the end of the M phase [23]. Debate continues about whether, and how, the cell cycle influences the rate of nanoparticle internalisation [23, 33, 34]. Additionally, the inclusion of multiple stages shifts the distribution of cell division times from an exponential distribution to a hypoexponential distribution, which has been shown to more accurately reflect experimental observations [32]. Note that the number of stages in the proliferation model do not necessarily correspond to the four stages in the cell cycle. In our model, an agent at proliferation stage p is randomly selected, with replacement, with probability P_p during a timestep of

duration τ. If $p \neq \Pi$, the agent simply progresses to the $p+1$th stage of the cell cycle [32]. If $p = \Pi$ the agent, located at $(x\Delta, y\Delta)$, attempts to place a daughter agent at a target site that is randomly selected from the four nearest-neighbour sites located at $(x\Delta \pm \Delta, y\Delta)$ and $(x\Delta, y\Delta \pm \Delta)$. Similar to motility events, a proliferation event will be successful if the target site is unoccupied, and will otherwise be aborted (Figure 1(f))[31]. If the event is successful, the proliferation stages of both the parent and daughter agent are set to $p = 1$. If the event is aborted, the agent remains in stage Π.

2.2. Nanoparticle internalisation model

To describe the internalisation of nanoparticles by the cell population, we implement a multistage stochastic process. That is, nanoparticles transition through stages $0 \leq s \leq S$, where stage 0 represents nanoparticles in the culture media and stage S represents fully internalised nanoparticles. We can select particular S values to represent specific models of internalisation. For example, $S = 1$ represents a single stage association model, whereas $S = 2$ represents a model of nanoparticle binding and internalisation. We initially impose a nanoparticle suspension that contains N_{initial} nanoparticles. We assume that these nanoparticles are uniformly distributed throughout the experimental domain, that is, that the suspension in the culture media is well-mixed. This assumption is appropriate provided that the media is continuously stirred or the nanoparticles are sufficiently small and/or light such that diffusion is the dominant component of nanoparticle motion [27]. Accordingly, in the model there are initially, on average, N_{initial}/XY nanoparticles in the media above each lattice site (Figure 1(c)).

During a timestep of duration τ, an individual nanoparticle in the media can bind to an agent with probability P_{bind}. This binding probability represents two processes. First, the nanoparticle must reach the cell layer during that timestep via random motion and an agent must be present on the relevant lattice site. Nanoparticle diffusivity arises from the Stokes-Einstein equation [26], and is given by

$$D = \frac{k_b T}{3\pi\eta d},$$

where k_b is the Boltzmann constant, T is the temperature of the media, η is the dynamic viscosity of the media and d is the nanoparticle diameter. The inverse relationship between nanoparticle diffusivity and diameter implies that smaller nanoparticles are more likely to arrive at the cell layer during a timestep. The second process is the nanoparticle binding to the cell, given that the nanoparticle has arrived at the cell layer. This occurs at a rate proportional to the strength of interaction, also known as the affinity, between the nanoparticle and the cell [19]. The probability that the nanoparticle arrives at the cell layer and binds to a cell during a timestep is a function of media depth, h, and nanoparticle diffusivity [35],

$$P_{\text{bind}} = \lambda_1 \tau = \beta \frac{D\pi\tau}{4h^2},$$

where $0 \leq \beta \leq 1$ is the probability that the nanoparticle binds to the cell, given it has arrived at the cell layer, and λ_1 is the rate parameter describing the transition from a nanoparticle in the fluid ($s = 0$) to a nanoparticle bound to a cell membrane ($s = 1$). Calculating this probability allows us to determine the rate of nanoparticle binding without explicitly tracking the locations of nanoparticles in the media.

The first stage of the internalisation process corresponds to nanoparticles binding to the cell membrane. Depending on the physicochemical properties of the nanoparticles and the cell phenotype, the nanoparticle can be internalised via a number of endocytic pathways. These pathways can involve macropinocytosis, receptor recruitment, formation of caveolae or membrane invaginations, and endosomal trafficking [4, 17]. Additionally, the pathway is not necessarily unidirectional, as nanoparticle-receptor binding is reversible and nanoparticle recycling (exocytosis) can occur. As, in general, these pathways are not fully characterised, we choose to represent internalisation as an S-stage stochastic process. We make the assumption that each stage of internalisation is a Poisson process, that is, progressing through the stage requires an exponentially-distributed amount of time. We denote the

rate parameter of the sth stage as λ_s, which represents the rate of transition from state $s-1$ to state s.

It has been demonstrated that cells have a finite carrying capacity for associated nanoparticles [19, 36]. It is unclear whether this bottleneck occurs due to a saturation of nanoparticles at the cell surface, or at the latter stages of internalisation. We account for this phenomenon by incorporating a maximum number of nanoparticles (i.e. a carrying capacity) at each stage of internalisation, K_s, and scaling the corresponding rate parameter by the available fraction of a cell's carrying capacity, giving an effective rate parameter of $\lambda_s^e(t) = (1 - N_s(t)/K_s)\lambda_s$, where $N_s(t)$ is the number of nanoparticles in the sth stage of internalisation at time t. The effective rate parameter reduces to the original rate parameter in the limit $K_s \to \infty$.

The model provides information about the number of nanoparticles in each internalisation stage for each agent in the population (Figures 1(m)-(r)). For the ith agent in the population, we denote the number of nanoparticles in each stage as $A_i = (N_1^i, N_2^i, \ldots, N_S^i)$. The number of associated nanoparticles for the ith agent is the sum of the entries in A_i. Nanoparticles are defined as internalised if they are in stage S. When an agent undergoes division, the nanoparticles in each internalisation stage for that agent are split between the parent and daughter agent according to a binomial process. Experimental evidence suggests that a daughter cell inherits between 52% and 72% of the associated nanoparticles [8, 20]. The remainder of the nanoparticles are associated with the parent cell such that the total number of associated nanoparticles is conserved. Accordingly, we randomly distribute the nanoparticles between the daughter and parent agent in the sth stage via a binomial process with N_s^i trials and a probability of inheritance I. The daughter agent is always defined as the agent that is placed at a neighbouring lattice site.

2.3. Model implementation

We perform all simulations of the model on a lattice with $X = 10$ and $Y = 10$ sites in the x and y directions, respectively. Initially, C_0 unique sites are selected at random and an agent is placed on each site. The cell cycle stage of each agent is selected uniformly at random. We use a fixed timestep approximation to simulate the evolution of the system in time [37]. In each timestep of duration τ we update the system according to three types of events: nanoparticle internalisation events, cell motility events, and cell proliferation events. For internalisation events, we keep track of the number of nanoparticles in each stage of internalisation for each agent in the simulation. We assume that nanoparticles are uniformly distributed throughout the culture media and hence, on average,

$$N_0(j\tau) = \frac{1}{XY}\left(N_{\text{initial}} - \sum_{i=1}^{C(j\tau)} \sum_{s=1}^{S} N_s^i(j\tau)\right),$$

are available in the media above each lattice site after $j \in \{\mathbb{N}_0 \mid j \leq t_{\text{end}}/\tau\}$ time steps, where $C(j\tau)$ is the number of agents occupying the lattice at the beginning of the jth timestep and t_{end} is the final experimental time point. For each nanoparticle in the $s-1$th stage of internalisation, progression to the next stage occurs with probability $\lambda_s^e(j\tau)\tau$. We select τ such that $\lambda_s\tau \ll 1$ (and $M \leq 1,\ P_p \leq 1\ \forall\ p$), so that it is unlikely that a nanoparticle will progress through more than one internalisation stage in a single timestep. We calculate the number of nanoparticles that progress between internalisation stages for all agents and stages, and then simultaneously update the state of the system. For motility events, $C(j\tau)$ agents are selected at random, with replacement, and attempt to undergo a motility event with probability M. After the motility events, an additional $C(j\tau)$ agents are selected at random, with replacement, to proceed to the next stage of the cell cycle or attempt to divide, as appropriate, with probability P_p, where p is the cell cycle stage of the selected agent. If the agent divides, the associated nanoparticles are divided between the parent and daughter agent according to the aforementioned binomial process. Recall that both cell motility and division events are only successful if the randomly-selected target site is unoccupied. A number of identically-prepared realisations of the model are performed to generate representative average behaviour; the number

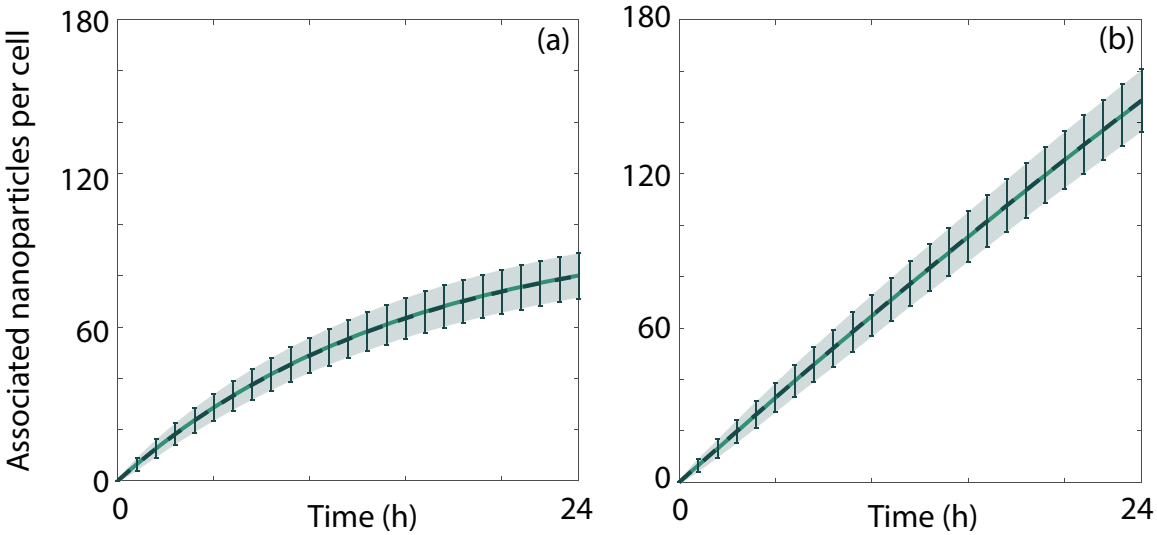

Figure 2: Comparison between the analytic and simulation predictions of the number of associated nanoparticles per cell at (a) full confluence and (b) 10% confluence. Lines correspond to the analytic (dashed) and simulation (solid) predictions of the mean. The analytic and simulation predictions of the mean $\pm$ one standard deviation correspond to the error bars and ribbons, respectively. Parameters used are $d = 20$ nm, $N_{\text{initial}} = 10^4$, $h = 5\times10^{-4}$ m, $\lambda_1 = 6.71\times10^{-2}$ h^{-1}, $P_p = 0\ \forall\ p$, $S = 1$, $K_1 \to \infty$, and (a) $C_0 = 100$, (b) $C_0 = 10$. All simulation data are obtained from 200 identically-prepared realisations of the simulation.

of realisations performed to obtain a specific result is presented in the relevant figure caption. All simulations are performed in Matlab R2020b and all code is available on GitHub. For all simulations we use $M = 1$, $\tau = 1/6$ h, $t_{\text{end}} = 24$ h, $T = 310$ K, $\eta = 1.0005\times10^{-3}$ kg m^{-1} s^{-1}, $k_b = 1.38\times10^{-23}$ m^2 kg s^{-2} K^{-1} and $\Delta = 25$ μm. Note that in the code M and P_p are calculated by defining an expected waiting time between motility and proliferation events, respectively.

3. Results and Discussion

We are interested in the distribution of $N_s(t)$ across the agent population, as this represents the dosage distribution for each stage of the internalisation process. Typically, it is not possible to obtain such information experimentally, as it is not straightforward to identify which stage of internalisation a nanoparticle is in [15]. However, as we will demonstrate, it is possible to obtain analytic results for the dosage distribution for each stage of internalisation under certain simplifying assumptions.

3.1. Nanoparticle association

The simplest form of the model that we consider is a single stage internalisation process for a cell population that is fully confluent. Here we will use the terminology of *associated* nanoparticles to highlight that there is no distinction between nanoparticles bound to the cell membrane and nanoparticles that have been internalised by the cell [19]. While this is an oversimplification of the internalisation process, it aligns with standard experimental practice [15]. As the cell population is fully confluent, no division events are possible, and nanoparticle inheritance can be neglected. We further assume that the impact of the carrying capacity can be neglected, that is, that $K_1 \to \infty$ and hence $\lambda_1^e(t) = \lambda_1$. Under these assumptions, the mean number of associated nanoparticles per cell by time t is

$$\mathbb{E}[N_1(t)] = \frac{N_{\text{initial}}}{XY}\left(1 - e^{-\lambda_1 t}\right), \tag{1}$$

which is the cumulative distribution function (CDF) of an exponential distribution with rate parameter λ_1, multiplied by the average number of nanoparticles initially present in the culture media above each lattice site. As this is simply an exponential process, the distribution of the number of associated nanoparticles per cell by time t is a Poisson distribution with rate parameter $N_{\text{initial}}(1 - e^{-\lambda_1 t})/XY$, a result that is consistent with previous studies [6, 7]. We present the mean and standard deviation of the number of associated nanoparticles per cell, obtained via simulation, alongside the mean and standard deviation of the Poisson distribution in Figure 2(a). We observe that the analytic predictions of the dosage distribution from Equation (1) matches that obtained from the simulation, both in terms of the mean and standard deviation of the number of associated nanoparticles per cell. The number of associated nanoparticles per cell increases approximately linearly at early time, and plateaus as the number of nanoparticles remaining in the media decreases.

In mathematical models, it is standard to assume that experiments are performed on fully confluent cell populations; however, in certain cases it is desirable to commence experiments before the cell population becomes fully confluent [23]. The cell population may or may not reach full confluence by the end of the experiment, and this information is not commonly reported. If the cell population is not fully confluent, then the total number of associated nanoparticles is necessarily reduced as it is possible for nanoparticles to arrive at the base of the culture dish without interacting with a cell. If we assume that the amount of cell proliferation over the course of the experiment is negligible, then the number of associated particles per cell at time t is Poisson distributed with rate parameter

$$\mathbb{E}[N_1(t)] = \frac{N_{\text{initial}}}{C_0}\left(1 - e^{-\lambda_1 C_0 t/XY}\right), \tag{2}$$

where $0 \leq C_0 \leq XY$ is the number of cells in the population. This can be considered as the CDF of an exponential random variable that represents the time taken for a nanoparticle to arrive at the bottom of the culture dish at a location where a cell resides, and to bind to that cell, multiplied by the number of initially available nanoparticles per cell. The rate parameter of the random variable, $\lambda_1 C_0/XY$, decreases with the level of confluence, reflecting that it is less likely for an individual nanoparticle to interact with a cell. While the rate parameter decreases, there is a corresponding increase in the maximum number of nanoparticles per cell (i.e. the number of nanoparticles in the initial suspension is constant but there are fewer cells). Interestingly, the combination of these two effects is that the mean number of associated nanoparticles per cell is approximately independent of confluence when only a small proportion of the nanoparticles are associated (i.e. when $\lambda_1 C_0 t/XY$ is small and we are in the linear association regime). We recover Equation (1) when $C_0 = XY$.

We present a comparison between the average simulation behaviour and the Poisson distribution for a cell population at 10% confluence in Figure 2(b). Again, we see that the simulated dosage distribution matches both the analytic mean and standard deviation of the number of associated nanoparticles per cell. Intuitively, the approximately linear behaviour continues for a significantly longer time compared to the fully confluent case as dosage depletion effects are not relevant over the 24 hours of the experiment, due to the reduced number of cells available.

If the cell population is not fully confluent initially, and cell proliferation cannot be neglected, it is not straightforward to obtain a closed-form analytic solution for the mean number of associated nanoparticles per cell. For a single stage model of cell proliferation (i.e. $\Pi = 1$), the mean number of cells in the population, $\overline{C}(t)$, is well-approximated by logistic growth, provided that the rate of cell motility is significantly higher than the rate of proliferation [31], and hence

$$\overline{C}(t) = \frac{XYC_0}{C_0 + (XY - C_0)e^{-\xi t}}, \tag{3}$$

where $\xi = P_1/\tau$ is the rate of cell proliferation. To the best of our knowledge, there is no analytic expression for the distribution of the number of cells in the population at time t. We can, however,

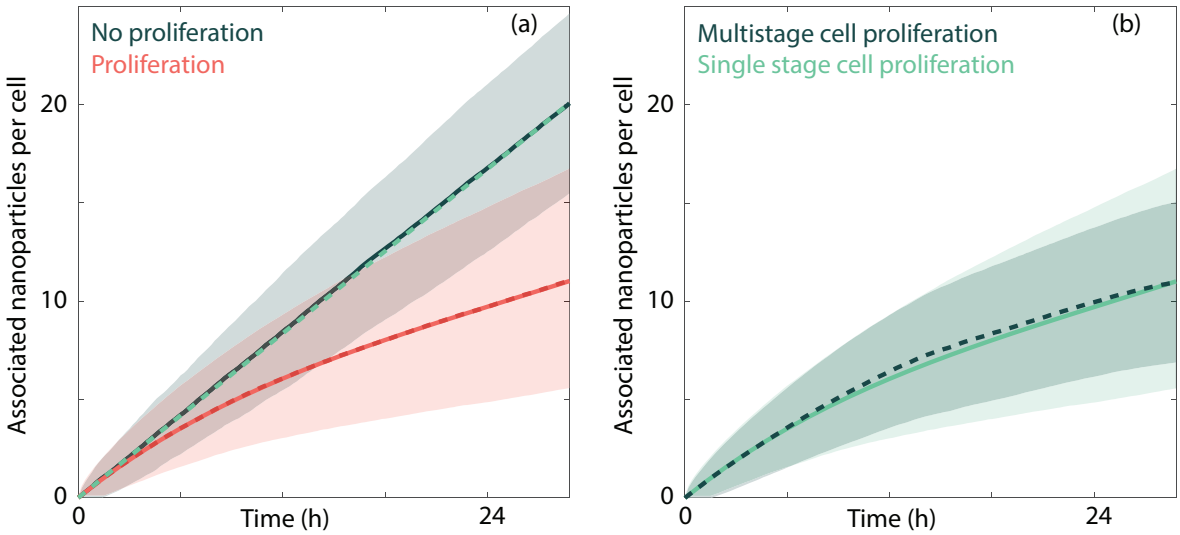

Figure 3: Comparison of the number of associated nanoparticles per cell for different proliferation models. (a) Comparison between no proliferation (green) and single stage proliferation (red) for analytic (dashed) and simulation (solid) predictions. (b) Comparison between single stage (light green, solid) and multistage proliferation (dark green, dashed) for simulation predictions. The ribbons correspond to the mean $\pm$ one standard deviation. Parameters used are $d = 50$ nm, $N_{\text{initial}} = 10^5$, $h = 5 \times 10^{-3}$ m, $\lambda_1 = 8.42 \times 10^{-4}$ h^{-1}, $S = 1$, $C_0 = 10$, $I = 0.7$, $K_1 \to \infty$, (a): $\Pi = 1$, $P_1 = 0$ (green), $P_1 = 1/72$ (red); (b): $\Pi = 1$ (light green), $P_1 = 1/72$ (light green), $\Pi = 24$ (dark green), $P_p = 1/3 \ \forall \ p$ (dark green). All simulation data are obtained from 1000 identically-prepared realisations of the simulation.

use Equation (3) to find an integral expression for the mean number of associated nanoparticles per cell in the presence of cell proliferation

$$\mathbb{E}[N_1(t)] = \frac{N_{\text{initial}}}{\overline{C}(t)} \int_0^t \lambda_1 \frac{\overline{C}(\tau)}{XY} e^{-\lambda_1 \overline{C}(\tau)\tau/XY} \, \mathrm{d}\tau. \tag{4}$$

Similar to Equation (2), this can be considered as the CDF of a random variable that represents the time required for a nanoparticle to arrive at, and bind to, a cell, multiplied by the number of initially available nanoparticles per cell. However, as the number of cells increases with time, we must account for the increased chance that a nanoparticle arrives at the base of the culture dish and interacts with a cell. In general, this expression cannot be evaluated analytically, and we are restricted to numerical integration methods.

We present a comparison between the mean number of associated nanoparticles per cell, as predicted by the simulation and obtained from numerically integrating Equation (4) for a cell population undergoing proliferation in Figure 3(a). We observe that the mean number of nanoparticles per cell decreases, compared to the case without proliferation. This result is expected, as the nanoparticles associated to a cell are split between the parent and daughter cell upon division. Further, we observe that the integral expression in Equation (4) accurately describes the mean number of nanoparticles per cell obtained from the simulation. The choice of proliferation model has a small influence on the mean number of associated nanoparticles per cell, as can be seen in Figure 3(b), where we compare simulation results obtained using either a single stage or multistage ($\Pi = 24$) model of proliferation. Instead, the influence of the proliferation model manifests in the spread of the dosage distribution. The multistage proliferation model results in a narrower dosage distribution, as the number of divisions per cell is more consistent across the population. We note that the level of asymmetry present in the inheritance process of associated nanoparticles does not affect the mean number of nanoparticles per cell, as the rate of association is independent of the number of previously-associated nanoparticles. However, the effect of the inheritance is observable in the dosage distributions, presented in Figure 4. The

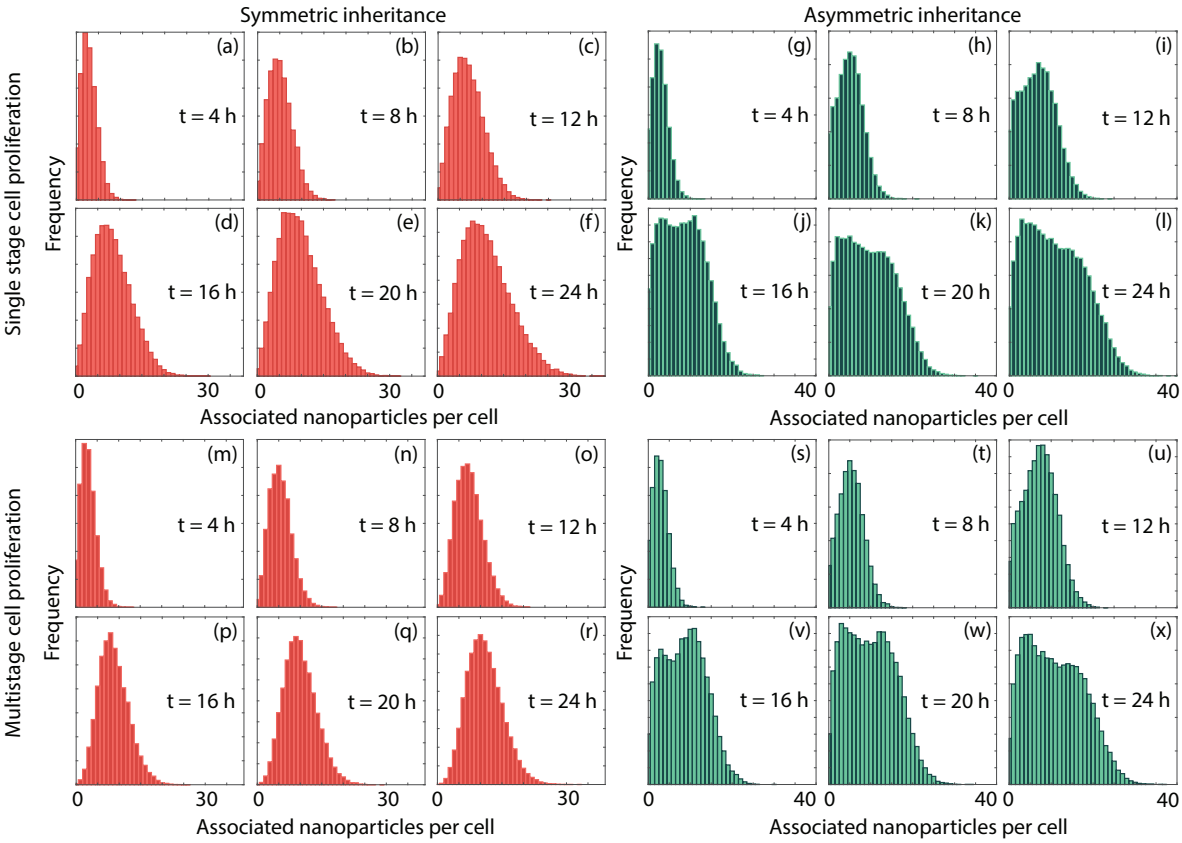

Figure 4: Dosage distributions recorded at four hour intervals for (a)-(f) single stage proliferation and symmetric inheritance, (g)-(l) single stage proliferation and asymmetric inheritance, (m)-(r) multistage proliferation and symmetric inheritance, and (s)-(x) multistage proliferation and asymmetric inheritance. Parameters used are $d = 50$ nm, $N_{\text{initial}} = 10^5$, $h = 5 \times 10^{-3}$ m, $\lambda_1 = 8.42 \times 10^{-4}$ h^{-1}, $S = 1$, $C_0 = 10$, $K_1 \to \infty$, (a)-(f), (m)-(r) $I = 0.5$, (g)-(l), (s)-(x) $I = 0.9$, (a)-(l): $\Pi = 1$, $P_1 = 1/72$; (m)-(x): $\Pi = 24$, $P_p = 1/3 \ \forall \ p$. All simulation data are obtained from 1000 identically-prepared realisations of the simulation.

distribution of associated nanoparticles per cell is noticeably broader if the inheritance is asymmetric (Figures 4(g)-(l) and 4(s)-(x)). In the asymmetric case, we observe that there is a substantial increase in the number of cells that have zero nanoparticles associated by 24 hours, which only occurs rarely for symmetric inheritance. We again observe that the dosage distribution is narrower for the multi-stage proliferation model (Figures 4(m)-(x)) than the single stage proliferation model (Figures 4(a)-(l)).

One benefit of employing the model is that it is possible to divide the population dosage distribution into separate dosage distributions based on the number of divisions a cell has experienced. That is, the population dosage distribution can be considered as a mixture distribution of the dosage distributions for cell subpopulations that have never divided, divided once, divided twice, and so on. Here we make the assumption that the cell population is not close to confluence, and hence the growth of the cell population is approximately exponential. Further, we make the assumption that dosage depletion effects can be neglected, that is, that we are in the regime where association is independent of confluence. We first consider the subpopulation of cells that have experienced division exactly once by time t, which includes both the parent and daughter cells. We define the time at which the cell undergoes division as t_1. Under the assumption of exponential growth, we know that t_1 is uniformly distributed on the finite interval $0 \leq t_1 \leq t$. This can be seen by defining two i.i.d. exponential random variables X_1 and X_2, which represent the time of the first and second divisions of a cell, and calculating $p(X_1 = t_1 | X_1 < t,\ X_1 + X_2 > t)$ for $0 \leq t_1 \leq t$. Accordingly, the dosage distribution of this subpopulation is a mixture distribution with two equally-weighted components: the dosage distribution of parent cells, which are Poisson distributed with rate parameter

$$\gamma_{\{\mathrm{p}\}}(t) = \frac{N_{\mathrm{initial}}}{XY}\left[(1-I)\left(1-e^{-\lambda_1 t_1}\right) + 1 - e^{-\lambda_1 (t-t_1)}\right],\ t_1 \sim U(0,t),$$

and the dosage distribution of the daughter cells, which are Poisson distributed with rate parameter

$$\gamma_{\{\mathrm{d}\}}(t) = \frac{N_{\mathrm{initial}}}{XY}\left[I\left(1-e^{-\lambda_1 t_1}\right) + 1 - e^{-\lambda_1 (t-t_1)}\right],\ t_1 \sim U(0,t),$$

recalling that I denotes the proportion of nanoparticles that are inherited by a daughter cell upon division. There are two components for each rate parameter: the number of particles that associated to the cell after division occurs, and the number of particles that associated before cell division, and remained after division. There will be, on average, an equal number of daughter and parent cells that have divided exactly once.

We follow a similar process to obtain the dosage distribution for the subpopulation of cells that have divided exactly twice by time t. We define the time at which the first and second divisions occur as t_1 and t_2. From order statistics [38], we know that the PDF of t_1 is

$$p(t_1) = \frac{2}{t}\left(1 - \frac{t_1}{t}\right),$$

which implies that

$$\frac{t_1}{t} \sim \mathrm{Beta}(1,2).$$

In turn, the time between the first and second division events, $t_2 - t_1$, is uniformly distributed on $0 \leq t_2 - t_1 \leq t - t_1$. There are four equally-weighted components in the subpopulation dosage mixture

distribution, which are Poisson distributed with rate parameters

$$\gamma_{\{\mathrm{p,p}\}}(t) = \frac{N_{\text{initial}}}{XY}\left[(1-I)^2\left(1-e^{-\lambda_1 t_1}\right) + (1-I)\left(1-e^{-\lambda_1(t_2-t_1)}\right) + 1 - e^{-\lambda_1(t-t_2)}\right],$$
$$\gamma_{\{\mathrm{p,d}\}}(t) = \frac{N_{\text{initial}}}{XY}\left[I(1-I)\left(1-e^{-\lambda_1 t_1}\right) + I\left(1-e^{-\lambda_1(t_2-t_1)}\right) + 1 - e^{-\lambda_1(t-t_2)}\right],$$
$$\gamma_{\{\mathrm{d,p}\}}(t) = \frac{N_{\text{initial}}}{XY}\left[(1-I)I\left(1-e^{-\lambda_1 t_1}\right) + (1-I)\left(1-e^{-\lambda_1(t_2-t_1)}\right) + 1 - e^{-\lambda_1(t-t_2)}\right],$$
$$\gamma_{\{\mathrm{d,d}\}}(t) = \frac{N_{\text{initial}}}{XY}\left[I^2\left(1-e^{-\lambda_1 t_1}\right) + I\left(1-e^{-\lambda_1(t_2-t_1)}\right) + 1 - e^{-\lambda_1(t-t_2)}\right],$$

where

$$\frac{t_1}{t} \sim \text{ Beta}(1,2),\ t_2 - t_1 \sim U(0, t-t_1),$$

and the subscript of $\gamma(t)$ indicates the order and type of division events experienced. For example the subscript {p,d} indicates that a cell has experienced two division events; the first of which where it was the parent cell and the second of which where it was the daughter cell. An increase in the asymmetry of inheritance corresponds to a larger difference between the rate parameters of each component of the mixture distribution, which can induce multimodality in the dosage distribution, as observed in Figure 4. If inheritance is symmetric (i.e. $I = 0.5$), the rate parameters for each component are identical and the dosage distribution is unimodal.

We can generalise this process to obtain the dosage distribution for the subpopulation of cells that have divided N times by time t, where the time of the nth division ($1 \leq n \leq N$) is denoted t_n. Again, from order statistics [38], the PDF for $t_n - t_{n-1}$ (i.e. the time between division events) is

$$p_n(t_n - t_{n-1}) = \frac{N-n+1}{t-t_{n-1}}\left(1 - \frac{t_n - t_{n-1}}{t - t_{n-1}}\right)^{N-n},$$

noting that we define $t_0 = 0$, and hence

$$\frac{t_n - t_{n-1}}{t - t_{n-1}} \sim \text{Beta}(1, N-n+1). \tag{5}$$

To obtain the general form of the rate parameters, we define the sequence $a_n = \{b_1, b_2, \cdots, b_n\}$, where $b_j \in \{\mathrm{d,p}\}$, which represents the order of the n division events that a cell has experienced, and whether it was the daughter (d) or parent (p) cell at each division. We define $\Omega_{\mathrm{d},i}$ and $\Omega_{\mathrm{p},i}$ as the number of times that a cell was the daughter cell or the parent cell, respectively, in the last i elements in the sequence. Accordingly, we define the rate parameter for an arbitrary sequence

$$\gamma_{a_n}(t) = \frac{N_{\text{initial}}}{XY}\left[1 - e^{-\lambda_1(t-t_n)} + \sum_{i=1}^{n} I^{\Omega_{\mathrm{d},i}}(1-I)^{\Omega_{\mathrm{p},i}}\left(1 - e^{-\lambda_1(t_{n-i+1}-t_{n-i})}\right)\right], \tag{6}$$

where t_i for $1 \leq i \leq n$ is obtained from a Beta distribution as defined in (5) and $t_0 = 0$. We note that there are 2^n permutations of the cell division sequence, and hence there are 2^n rate parameters for the cell subpopulation that has experienced n divisions and the corresponding mixture distribution has 2^n components.

We now highlight the validity of this approximate dosage distribution for each cell subpopulation. In Figures 5(a)-(f), we present the dosage distribution for the entire cell population, obtained from the simulation. We observe the asymmetry in the distribution that arises from the asymmetric inheritance process. We next separate the dosage distribution into its constituent components of the dosage

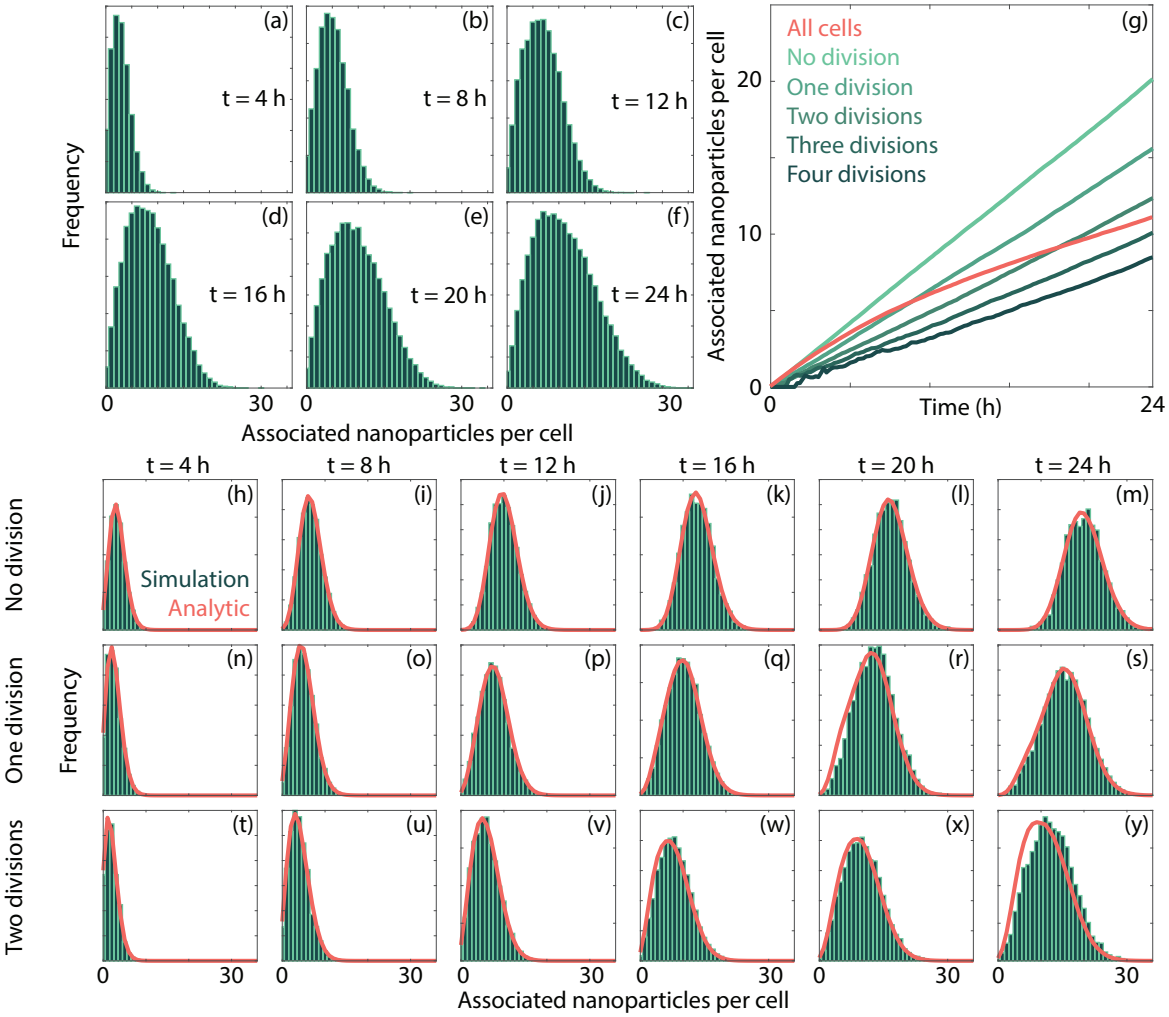

Figure 5: Dosage distributions for subpopulations of cells based on the number of divisions that a cell has experienced. (a)-(f) Dosage distributions recorded at four hour intervals for the entire cell population. (g) Mean number of associated nanoparticles per cell for each cell subpopulation. (h)-(y) Comparison between the analytic (solid line) and simulation (histogram) predictions of the dosage distribution for cells that have experienced (h)-(m) zero, (n)-(s) one, and (t)-(y) two cell divisions recorded at four hour intervals. Parameters used are $d = 50$ nm, $N_{\text{initial}} = 10^5$, $h = 5 \times 10^{-3}$ m, $\lambda_1 = 8.42 \times 10^{-4}$ h^{-1}, $S = 1$, $C_0 = 10$, $I = 0.7$, $\Pi = 1$, $P_1 = 1/72$, $K_1 \to \infty$. Analytic predictions are constructed from 10^6 samples of the mixture distribution. All simulation data are obtained from 1000 identically-prepared realisations of the simulation.

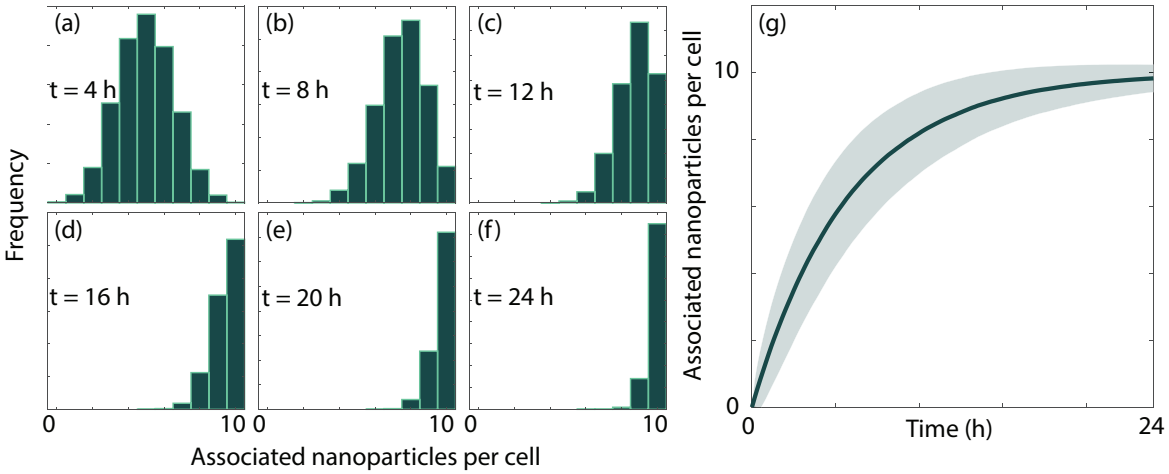

Figure 6: Dosage distributions for cells with a finite carrying capacity of nanoparticles. (a)-(f) Dosage distributions recorded at four hour intervals obtained from the simulation. (g) Mean ($\pm$ one standard deviation) number of associated nanoparticles per cell obtained from the simulation. Parameters used are $d = 50$ nm, $N_{\text{initial}} = 10^5$, $h = 3 \times 10^{-3}$ m, $\lambda_1 = 1.70 \times 10^{-3}$ h^{-1}, $S = 1$, $C_0 = 100$, $K_1 = 10$. All simulation data are obtained from 1000 identically-prepared realisations of the simulation.

distribution for cell subpopulations (Figure 5(g)) that contain cells that have experienced division a specific number of times, and present these distributions for zero, one, and two divisions in Figures 5(h)-(y). As expected, we observe that cells that have experienced fewer divisions are associated to more nanoparticles. Interestingly, while the increase in the mean number of associated nanoparticles per cell is nonlinear, the increase in the mean number of associated nanoparticles per cell for each subpopulation is approximately linear. This implies that the apparent plateau in nanoparticle association can be attributed to cell division rather than dosage depletion effects. We also present the dosage distributions obtained from sampling from the mixture distributions defined via (5)-(6). We observe that the mixture distributions match the simulation results well. However, the approximation of the mixture distribution becomes less accurate as both time and the number of divisions increase. This is because the assumption of exponential growth becomes less appropriate as the number of cells in the population increases.

Thus far, we have considered a simplified scenario where the rate of nanoparticle association does not depend on the number of previously-associated nanoparticles. While this is appropriate in certain circumstances, such as for highly phagocytic cell species [19], previous investigations have demonstrated that the nanoparticle association process can become saturated for a sufficiently high administered nanoparticle dose. This implies that the rate of nanoparticle association decreases with the number of associated nanoparticles [19]. Saturation is attributed to a finite carrying capacity of individual cells, where there is a maximum number of associated nanoparticles per cell. To capture this scenario, we now apply a finite K_1 value, which enforces a decrease in the effective rate parameter $\lambda_1^e(t)$ as the number of associated nanoparticles increases. We present the dosage distributions obtained from the simulation with a finite carrying capacity in Figure 6. We observe that at early times, where the mean number of associated nanoparticles is small compared to the carrying capacity, the dosage distribution is approximately Poisson distributed (Figure 6(a)). However, as the mean number of associated nanoparticles approaches the carrying capacity, we observe that the dosage distribution becomes primarily located at the carrying capacity (Figure 6(f)). As such, the assumption of a Poisson dosage distribution is not always appropriate, as observed previously [6]. In Figure 6(g) we see that the standard deviation of the dosage distribution decreases as the mean number of associated nanoparticles approaches the carrying capacity, as opposed to the monotone increase that is expected if the dosage

is Poisson distributed. This highlights the benefit of employing the modelling framework to generate predictions of the dosage distribution, as it is not always possible to rely on analytic results, and the inclusion of specific biological mechanisms can influence the features of the dosage distribution.

3.2. Nanoparticle binding and internalisation

To now, we have focused on a single stage model of nanoparticle internalisation. In reality, the nanoparticle internalisation process is significantly more complicated than can be captured by a single stage model. The reason such simple models see widespread usage is that it is uncommon to measure the relevant experimental information necessary to distinguish between the stages of internalisation, and hence more complicated models can rarely be parameterised. Further details can found in the review of Fitzgerald and Johnston [15], who discuss the benefits and drawbacks of the various experimental techniques that can be used to distinguish between nanoparticles that are strongly bound to a cell's membrane, and those that have been internalised, such as in Figures 1(g)-(l). However, it is still instructive to consider how the number of nanoparticles in each stage of the internalisation process changes over time, under certain assumptions.

We next consider a two stage model, where nanoparticles first bind to a cell's membrane and, subsequently, become internalised by that cell. We assume that the cell population is fully confluent and that the carrying capacity at each stage of internalisation can be neglected. For a nanoparticle to be bound to a cell at time t, we require that the time of binding is less than t and that the time of internalisation is greater than t. If these two events occur according to two exponential random variables X_1 and X_2 with rates λ_1 and λ_2, then the probability that an individual nanoparticle is bound at time t is equivalent to $P(X_1 < t, X_1 + X_2 > t)$. Accordingly, the mean number of bound nanoparticles per cell is

$$\mathbb{E}[N_1(t)] = \frac{N_{\text{initial}}}{XY} \int_0^t \lambda_1 e^{-\lambda_1 \tau} e^{-\lambda_2 (t-\tau)} \, \mathrm{d}\tau = \frac{N_{\text{initial}}}{XY} \frac{\lambda_1}{\lambda_2 - \lambda_1} \left(e^{-\lambda_1 t} - e^{-\lambda_2 t} \right). \tag{7}$$

For a nanoparticle to be internalised at time t, we require that the combined binding and internalisation time is less than t, that is, $P(X_1 + X_2 < t)$. Hence the mean number of internalised nanoparticles per cell is

$$\mathbb{E}[N_2(t)] = \frac{N_{\text{initial}}}{XY} \int_0^t \lambda_1 e^{-\lambda_1 \tau} \left(1 - e^{-\lambda_2 (t-\tau)} \right) \mathrm{d}\tau = \frac{N_{\text{initial}}}{XY} \left(1 - \frac{\lambda_2}{\lambda_2 - \lambda_1} e^{-\lambda_1 t} + \frac{\lambda_1}{\lambda_2 - \lambda_1} e^{-\lambda_2 t} \right), \tag{8}$$

which is the CDF of a hypoexponential random variable with parameters λ_1 and λ_2 [39], multiplied by the average number of nanoparticles initially present in the culture media above each lattice site. The dosage distributions for bound and internalised nanoparticles, under the aforementioned assumptions, are Poisson distributions with rate parameters $\mathbb{E}[N_1(t)]$ and $\mathbb{E}[N_2(t)]$, respectively. These results can be extended to incorporate cell populations that are not at confluence, where

$$\mathbb{E}[N_1(t)] = \frac{N_{\text{initial}}}{C_0} \frac{C_0 \lambda_1}{XY\lambda_2 - C_0 \lambda_1} \left(e^{-\lambda_1 C_0 t / XY} - e^{-\lambda_2 t} \right),$$

and

$$\mathbb{E}[N_2(t)] = \frac{N_{\text{initial}}}{C_0} \left(1 - \frac{XY\lambda_2}{XY\lambda_2 - C_0 \lambda_1} e^{-C_0 \lambda_1 t / XY} + \frac{C_0 \lambda_1}{XY\lambda_2 - C_0 \lambda_1} e^{-\lambda_2 t} \right).$$

As for the single stage internalisation model, the effective rate parameter for binding decreases with confluence, but this is countered by the increase in the number of nanoparticles available to an individual cell, as the total number of nanoparticles in the culture media is constant.

We present a comparison between the analytic and simulation predictions of the dosage distribution for associated, bound, and internalised nanoparticles in Figure 7. The number of associated nanoparticles is the sum of the number of bound and internalised nanoparticles. We observe that the analytic

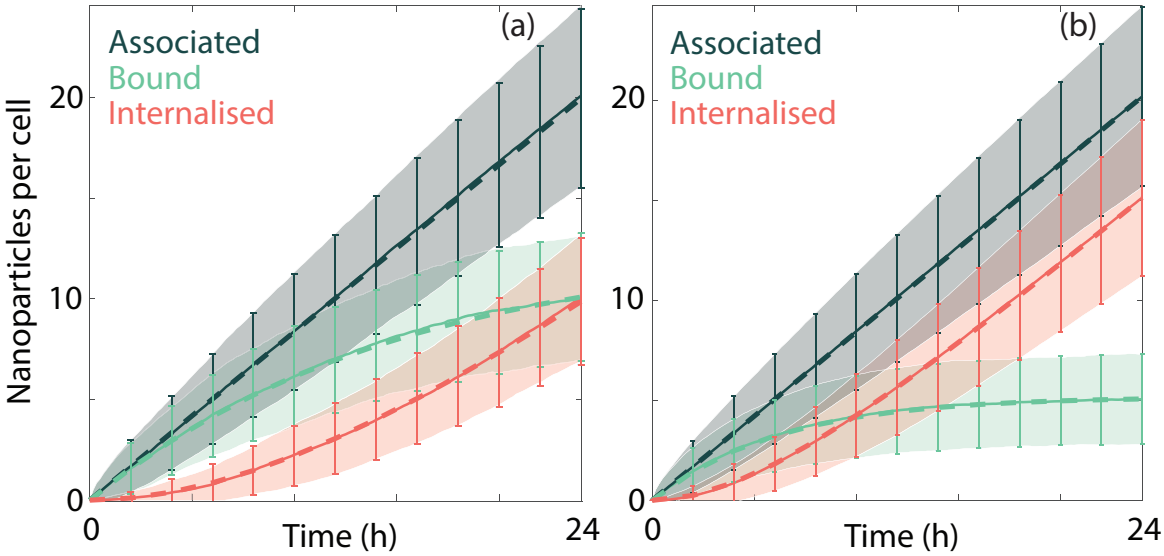

Figure 7: Comparison between the analytic and simulation predictions of the number of associated (dark green), bound (light green) and internalised (red) nanoparticles per cell at (a) full confluence and (b) 10% confluence. Lines correspond to the analytic (dashed) and simulation (solid) predictions of the mean. The analytic and simulation predictions of the mean $\pm$ one standard deviation correspond to the error bars and ribbons, respectively. Parameters used are $S = 2$, $K_1 \to \infty$, $K_2 \to \infty$, $N_{\text{initial}} = 10^5$, $\lambda_1 = 8.40 \times 10^{-4}$ h^{-1}, (a): $d = 50$ nm, $h = 5 \times 10^{-3}$ m, $\lambda_2 = 6.49 \times 10^{-2}$ h^{-1}, $C_0 = 100$; (b): $P_p = 0 \ \forall \ p$, $d = 20$ nm, $h = 3 \times 10^{-3}$ m, $\lambda_2 = 1.62 \times 10^{-1}$ h^{-1}, $C_0 = 10$. All simulation data are obtained from 500 identically-prepared realisations of the simulation.

predictions accurately describe the dosage distribution arising from the simulation, both in the case where the cell population is fully confluent (Figure 7(a)) and where the cell population is not fully confluent (Figure 7(b)). Further, these results highlight the importance of accurately distinguishing between bound and internalised nanoparticles [40], rather than reporting the number of associated nanoparticles. We see similar trends in nanoparticle association between Figures 7(a) and 7(b). However, the ratio of bound to internalised nanoparticles varies substantially due to the difference in the ratio of the binding and internalisation rate parameters. If the effective treatment of a cell relies on a threshold dose of nanoparticles being internalised, then we may observe a distinct response to the treatment, even though the number of associated nanoparticles is similar.

It is possible to calculate the mean number of nanoparticles per cell for each stage of the internalisation process for an arbitrary number of stages in the absence of any carrying capacities. While we state the result here, we note that it would be exceedingly difficult to parameterise a model with more than two stages from the types of experimental data that are routinely collected, and hence we do not focus on analysing simulation results for $S > 2$ here. The number of nanoparticles that have reached the Sth stage of internalisation (i.e. that have been internalised) at time t is

$$\mathbb{E}[N_S(t)] = \frac{N_{\text{initial}}}{XY}\left[1 - \sum_{j=1}^{S}\left(\prod_{i=1, i\neq j}^{S} \frac{\lambda_i}{\lambda_i - \lambda_j}\right)e^{-\lambda_j t}\right],$$

which arises from an S-stage hypoexponential distribution [39]. We can use this result to recursively define the number of nanoparticles in the sth stage of internalisation at time t for $1 \leq s \leq S-1$, as the number of nanoparticles in the sth stage is the difference between the number of nanoparticles

that have reached the sth and $(s+1)$th stages of internalisation

$$\mathbb{E}[N_s(t)] = \frac{N_{\text{initial}}}{XY}\left[1 - \sum_{j=1}^{s}\left(\prod_{i=1, i\neq j}^{s} \frac{\lambda_i}{\lambda_i - \lambda_j}\right)e^{-\lambda_j t} - \mathbb{E}\big[N_{s+1}(t)\big]\right]. \tag{9}$$

We note that we can describe cell populations that are not fully confluent via a rescaling of λ_1 and the number of nanoparticles available to each cell by XY/C_0 as previously. In the absence of a carrying capacity and cell proliferation, the dosage distribution for the sth stage of internalisation is a Poisson distribution with rate parameter $\mathbb{E}[N_s(t)]$.

If cell proliferation cannot be neglected, a Poisson dosage distribution is no longer appropriate. As in the case of the single stage internalisation model, it is possible to predict the dosage distribution by considering subpopulations of cells based on the number of division events that a cell has experienced. Again, we require that dosage depletion effects can be neglected, and that the initial confluency of the cell population is small. The distribution of cell division times is Beta distributed as defined in (5). For cells that have divided exactly once, the distribution of the number of bound nanoparticles per cell is a mixture distribution of equally-weighted two Poisson distributions with rate parameters

$$\gamma^1_{\{\text{p}\}}(t) = \frac{N_{\text{initial}}}{XY}\Big[(1-I)\mathbb{E}[N_1(t_1)] + \mathbb{E}[N_1(t-t_1)]\Big],$$
$$\gamma^1_{\{\text{d}\}}(t) = \frac{N_{\text{initial}}}{XY}\Big[I\mathbb{E}[N_1(t_1)] + \mathbb{E}[N_1(t-t_1)]\Big],$$

where $t_1 \sim U(0,t)$, $\mathbb{E}[N_1(t)]$ is defined in Equation (7), and the superscript denotes that the rate parameters correspond to the first stage of the internalisation process. The distribution of the number of internalised nanoparticles per cell is a mixture distribution of two equally-weighted Poisson distributions with rate parameters

$$\gamma^2_{\{\text{p}\}}(t) = \frac{N_{\text{initial}}}{XY}\Big[(1-I)\mathbb{E}[N_2(t_1)] + \mathbb{E}[N_2(t-t_1)]\Big],$$
$$\gamma^2_{\{\text{d}\}}(t) = \frac{N_{\text{initial}}}{XY}\Big[I\mathbb{E}[N_2(t_1)] + \mathbb{E}[N_2(t-t_1)]\Big],$$

where $t_1 \sim U(0,t)$, $\mathbb{E}[N_2(t)]$ is defined in Equation (8), and the superscript denotes that the rate parameters correspond to the second stage of the internalisation process.

We can express the components of the mixture distribution that represents the dosage of nanoparticles in the sth stage of internalisation for the subpopulation of cells that have experienced n divisions in general terms. Recall that $a_n = \{b_1, b_2, \cdots, b_n\}$, where $b_j \in \{\text{d,p}\}$, defines the number, order, and type of division events that a cell has experienced. The mixture distribution for the subpopulation of cells that have experienced exactly n divisions has 2^n equally-weighted components, each of which is a Poisson distribution with rate parameter

$$\gamma^s_{a_n}(t) = \frac{N_{\text{initial}}}{XY}\left[\mathbb{E}\big[N_s(t-t_n)\big] + \sum_{i=1}^{n} I^{\Omega_{\text{d},i}}(1-I)^{\Omega_{\text{p},i}}\Big(\mathbb{E}\big[N_s(t_{n-i+1}-t_{n-i})\big]\Big)\right], \tag{10}$$

where t_i for $1 \leq i \leq n$ is obtained from a Beta distribution as defined in (5), $t_0 = 0$, $\mathbb{E}\big[N_s(t)\big]$ is defined in Equation (9), $\Omega_{\text{d},i}$ and $\Omega_{\text{p},i}$ are the number of times that a cell was the daughter cell or the parent cell, respectively, in the last i elements in the sequence a_n. While this mixture distribution is not presented in a closed form, it allows us to efficiently sample from the dosage distribution at a particular time without performing realisations of the simulation.

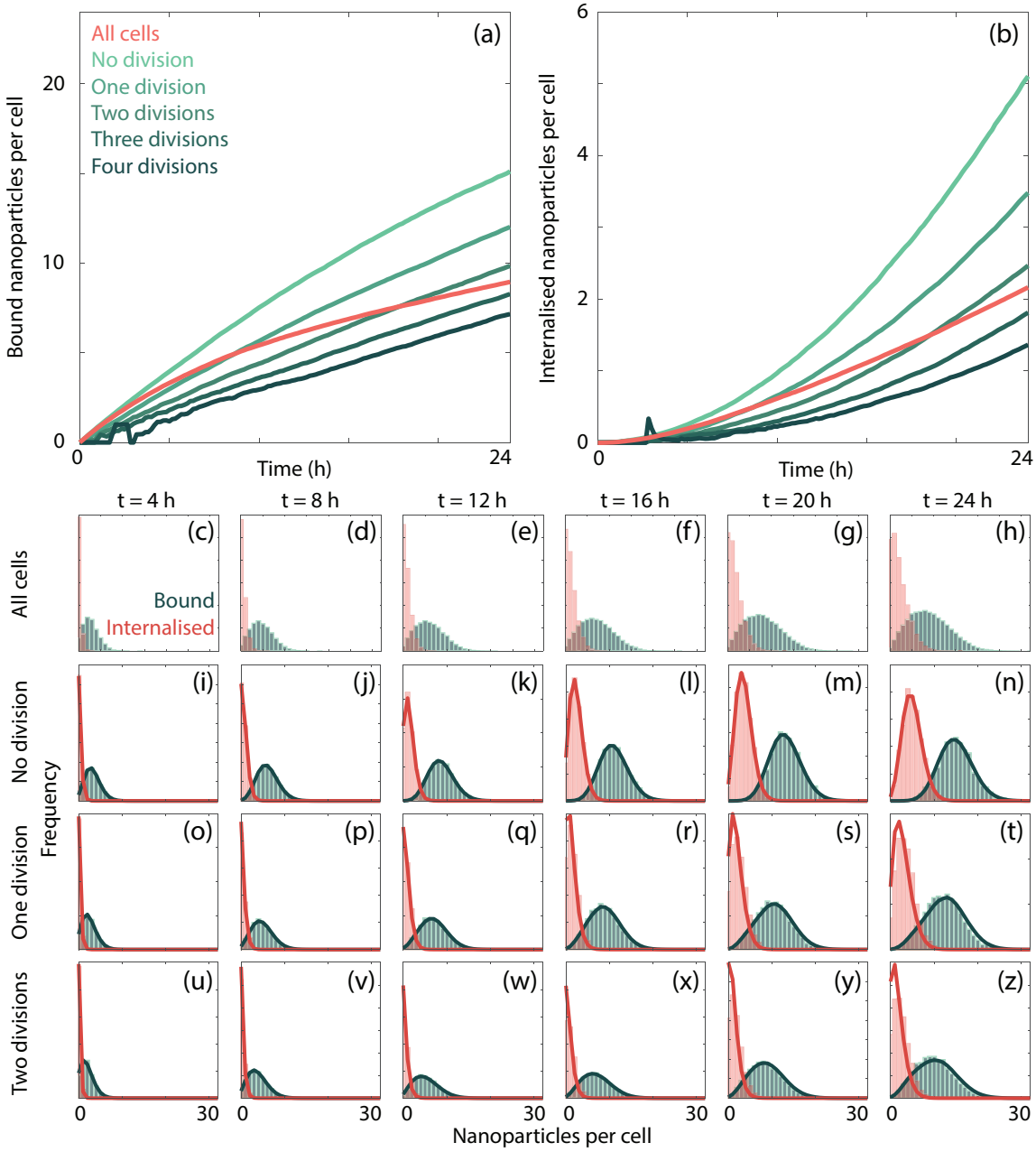

Figure 8: Dosage distributions of bound and internalised nanoparticles for subpopulations of cells based on the number of divisions that a cell has experienced. (a)-(b) Mean number of (a) bound and (b) internalised nanoparticles per cell for each cell subpopulation. (c)-(h) Dosage distributions for bound (green) and internalised (red) nanoparticles recorded at four hour intervals for the entire cell population. (i)-(z) Comparison between the analytic (solid line) and simulation (histogram) predictions of the dosage distribution for bound (green) and internalised (red) nanoparticles for cells that have experienced (i)-(n) zero, (o)-(t) one, and (u)-(z) two cell divisions recorded at four hour intervals. Parameters used are $d = 25$ nm, $N_{\text{initial}} = 10^5$, $h = 5 \times 10^{-3}$ m, $S = 2$, $\lambda_1 = 8.42 \times 10^{-4}$ h^{-1}, $\lambda_2 = 2.52 \times 10^{-2}$, $C_0 = 10$, $I = 0.7$, $\Pi = 1$, $P_1 = 1/72$, $K_1 \to \infty$. Analytic predictions are constructed from 10^6 samples of the mixture distribution. All simulation data are obtained from 1000 identically-prepared realisations of the simulation.

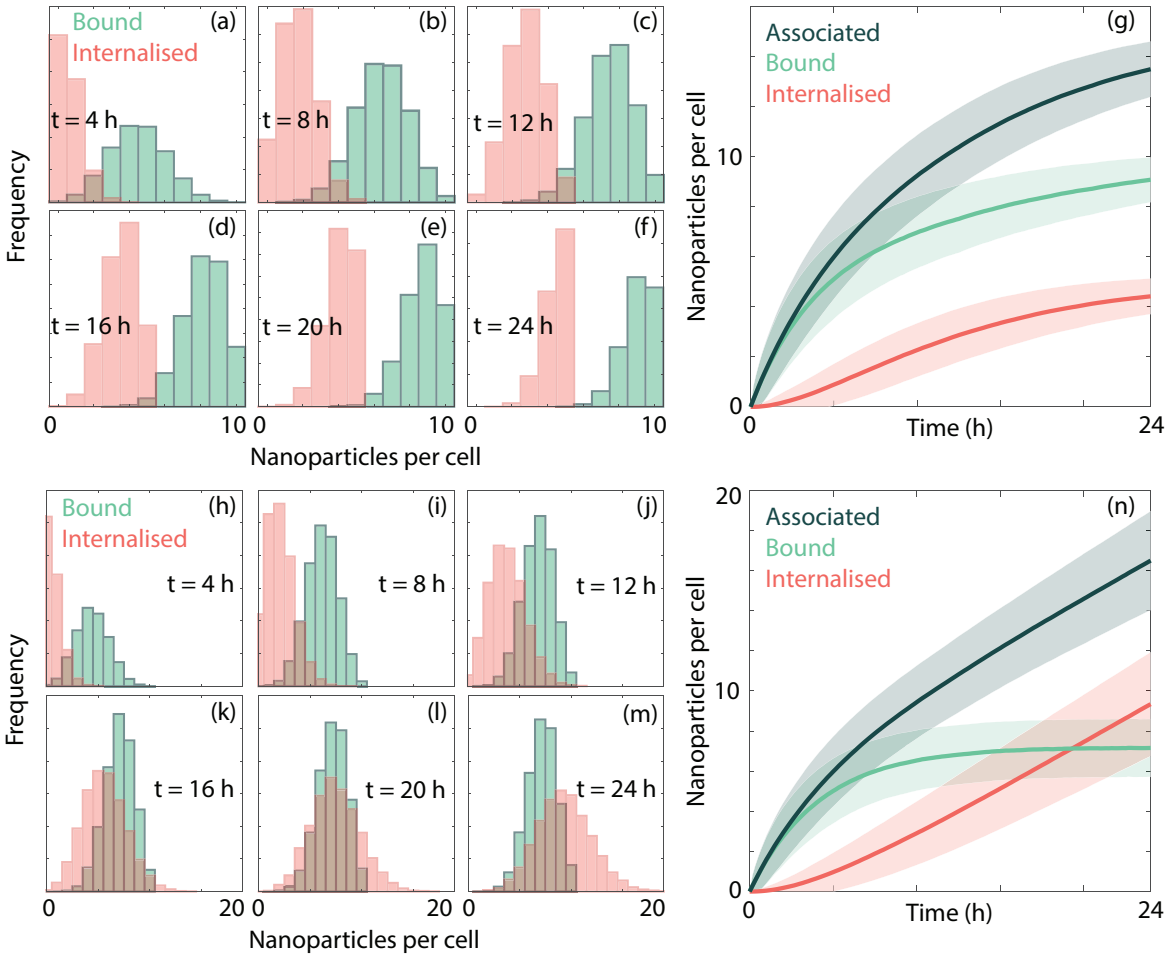

Figure 9: (a)-(f), (h)-(m) Dosage distributions recorded at four hour intervals for bound (green) and internalised (red) nanoparticles for cells with a finite carrying capacity of nanoparticles, obtained from the simulation. (g),(n) Mean ($\pm$ one standard deviation) number of associated (dark green), bound (light green) and internalised (red) nanoparticles per cell obtained from the simulation. Parameters used are $d = 50$ nm, $N_{\text{initial}} = 10^5$, $h = 3 \times 10^{-3}$ m, $S = 2$, $\lambda_1 = 1.70 \times 10^{-3}$ h^{-1}, $\lambda_2 = 6.58 \times 10^{-2}$ h^{-1}, $C_0 = 100$, (a)-(g): $K_1 = 10$, $K_2 = 5$; (h)-(n): $K_1 = 10$, $K_2 \to \infty$. All simulation data are obtained from 1000 identically-prepared realisations of the simulation.

We present a comparison of the mixture distribution and the dosage distribution arising from the simulation for a two stage internalisation model in Figure 8. We first present the mean number of bound and internalised nanoparticles per cell in Figures 8(a)-(b), respectively, both for the entire cell population, and for cell subpopulations separated based on the number of division events experienced. Again, we observe that cells that have experienced more division events have fewer bound and internalised nanoparticles. We present the dosage distributions for bound and internalised nanoparticles for cells that have experienced zero, one and two divisions in Figures 8(i)-(z). We see that the mixture distributions accurately approximate the dosage distributions obtained from the simulation. There are minor discrepancies between the mixture distributions and the simulation dosage distributions that appear as the number of cells in the population increases and the approximation of exponential growth is less accurate. However, as obtaining a sample from the mixture distribution for cells that have experienced n divisions only requires sampling $n+1$ random variables, it is significantly more efficient to use the mixture distributions to predict the dosage distribution across each of the cell subpopulations.

Previous investigations have highlighted the importance of modelling nanoparticle association as a saturating process [19]. However, it is not always obvious which stages of the internalisation process exhibit this saturation. For example, it is possible that a cell expresses a finite number of receptors that nanoparticles bind to in sufficient numbers such that there are no free receptors for further nanoparticle binding. Alternatively, cells have a finite internal volume available to be filled by nanoparticles, after which no further internalisation may occur, which may explain the saturation in nanoparticle association. To account for these possibilities we now introduce a finite carrying capacity for each stage of the internalisation process.

We consider two possible scenarios to examine the influence of finite carrying capacities. First, we consider the case where the rates of both nanoparticle binding and nanoparticle internalisation decrease with the number of previously bound and internalised nanoparticles, respectively. We present the dosage distributions for bound and internalised nanoparticles, obtained from the simulation, as well as the mean number of associated, bound and internalised nanoparticles per cell in Figures 9(a)-(g). Here we select $K_1 = 10$ and $K_2 = 5$, that is, at most ten nanoparticles can be bound to an individual cell and, at most, five nanoparticles can be internalised by a cell. We see that the carrying capacities result in dosage distributions that are not Poisson, particularly as the number of bound/internalised nanoparticles approaches the relevant carrying capacity. As expected, the mean number of bound and internalised nanoparticles per cell both plateau as the carrying capacities are approached, which is reflected in a corresponding plateau in the mean number of associated nanoparticles per cell. In the second case, only the rate of nanoparticle binding decreases with the number of previously bound nanoparticles. Here we choose $K_1 = 10$ and $K_2 \to \infty$. In the dosage distributions obtained from the simulation, presented in Figures 9(h)-(n), we see that the level of asymmetry in the number of bound nanoparticles is reduced, compared to the case with two carrying capacities. This is because it is always possible for a nanoparticle to transition from bound to internalised, and hence we do not see a buildup in the bound nanoparticle dosage distribution located at the carrying capacity. The dosage distribution for the internalised nanoparticles is approximately symmetric, and is more consistent with dosage distributions obtained in the absence of any carrying capacities. Interestingly, while we see a distinct plateau in the number of bound nanoparticles per cell, the fact that the number of internalised nanoparticles per cell is free to increase means that the number of associated nanoparticles per cell continues to increase. There is a qualitative difference in the shape of the nanoparticle association curves: the presence of both carrying capacities results in a plateau, compared to a single carrying capacity for the bound nanoparticles, which results in an initial decrease in the rate of association as the number of bound nanoparticles per cell plateaus, followed by a constant increase in the number of associated nanoparticles per cell. This implies that it may be possible to develop an experimental protocol that distinguishes between scenarios where carrying capacities may or may not be relevant, even if the number of bound and internalised nanoparticles cannot be (or are not) distinguished in the experimental data.

3.3. Model identification and parameter estimation

The modelling framework presented here can provide predictions about heterogeneity in nanoparticle dosage, based on assumptions about the biological mechanisms that are relevant for a particular experimental design. However, the questions of whether the presence of key biological mechanisms can be identified from standard experimental data [15], and the corresponding parameters estimated, remain open. While these questions merit an in-depth investigation, here we highlight certain cases where parameter estimation is possible, via both heuristic and numerical approaches. These approaches are informed by the form of the analytic results presented here. Further, we identify cases where it is not possible to distinguish between putative biological mechanisms using standard experimental data, motivating potential changes to experimental protocols.

A key parameter that informs the efficacy of a potential nanoparticle-based therapeutic is the nanoparticle-cell affinity [19]. This parameter provides a quantitative estimate of the strength of

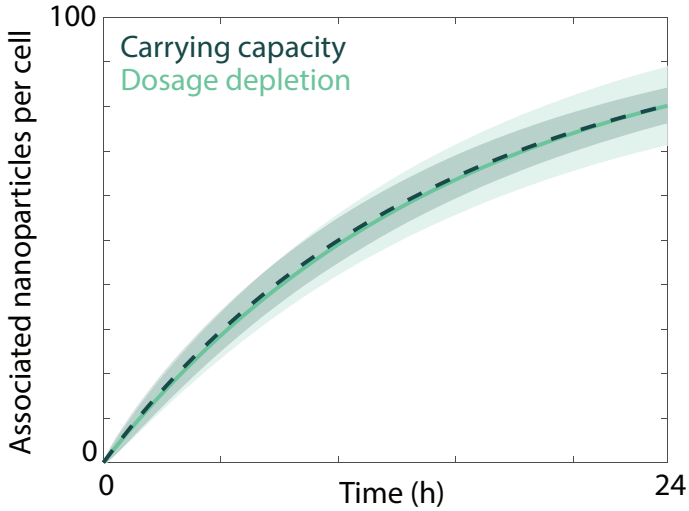

Figure 10: Comparison between the number of associated nanoparticles per cell obtained from the simulation for two saturating mechanisms: a finite carrying capacity (dark green, dashed) and depletion of nanoparticles in the culture media (light green, solid). Ribbons correspond to the mean ± one standard deviation. Parameters used are $d = 20$ nm, $h = 5 \times 10^{-4}$ m, $S = 1$, $C_0 = 100$, (light green): $\lambda_1 = 6.71 \times 10^{-2}$ h^{-1}, $N_{\text{initial}} = 10^4$, $K_1 \to \infty$; (dark green): $\lambda_1 = 7.075 \times 10^{-3}$ h^{-1}, $N_{\text{initial}} = 10^5$, $K_1 = 100$. All simulation data are obtained from 200 identically-prepared realisations of the simulation.

interaction between nanoparticles and cells [19]. In the context of the model presented here, the nanoparticle-cell affinity is proportional to λ_1. While this parameter can be estimated for each case where an analytic result is presented via numerical nonlinear curve fitting methods, provided that $\overline{N}_s(t)$ is measured for all s, where the bar indicates that this is the mean of the experimental data, such methods can require specialist knowledge to implement. Although such an approach would be preferable, here we discuss heuristic approaches for estimating key biological parameters, which require less specialised knowledge. For example, from the result in Equation (1), we know that at early experimental time points we should observe that the rate of nanoparticle association is approximately linear, with the caveat that there is negligible cell division and a high carrying capacity. Accordingly, λ_1 can simply be estimated via the slope of nanoparticle association over time. This result can be extended for multistage internalisation processes, as λ_1 can still be estimated from nanoparticle association data. Provided that $\overline{N}_s(t)$ is measured for all s and we have an estimate of λ_1, other transition rates can be estimated heuristically from the data. For example, for a two-stage internalisation process, we can estimate

$$\hat{\lambda}_2 = \frac{\hat{\lambda}_1 \frac{N_{\text{initial}}}{XY} - \frac{1}{\Delta t}\left(\overline{N}_1(t+\Delta t) - \overline{N}_1(t)\right)}{\overline{N}_1(t)},$$

where $\hat{\lambda}_1$ and $\hat{\lambda}_2$ are the estimated internalisation rate parameters. The estimate $\hat{\lambda}_2$ is obtained from the expected change in the number of bound particles between observations captured at a time Δt apart. Similar processes can be followed to estimate the rate parameters for other internalisation stages, provided the appropriate $\overline{N}_s(t)$ is measured experimentally. However, we note that this approach relies on derivatives estimated from experimental data via finite difference approximations, which may not be appropriate in the presence of substantial experimental noise [41].

Finally, we highlight pitfalls that can occur when attempting to identify the biological mechanisms that dictate nanoparticle internalisation. We present the mean number of associated nanoparticles per cell for two scenarios in Figure 10. The first scenario is where the cell population exhibits a saturating

Mechanism	Increased confluence	Cell proliferation	Asymmetric inheritance	Multistage internalisation	Carrying capacity	Cell cycle
Effect	Enhanced dosage depletion	Reduced uptake, broader dosage distribution	Multimodal, broader dosage distribution	Maintains Poisson dosage distribution	Narrower dosage distribution	Narrower dosage distribution
Analytic results	Yes	Yes	Yes	Yes	No	No

Table 1: Summary of the impact of specific biological mechanisms on the nanoparticle dosage distribution, and whether analytic results can be used to calculate the corresponding dosage distribution.

ability to associate with nanoparticles, that is, that a finite carrying capacity is present. The second scenario is where there is no carrying capacity, but the nanoparticles associate sufficiently rapidly over the course of the experiment that dosage depletion effects are relevant. As we observe in Figure 10, it is difficult to distinguish between the mean number of associated nanoparticles per cell for these two scenarios, as both cases exhibit a similar plateau. If the experimental data is reported in terms of either arbitrary fluorescence, a common approach [40], or the fluorescence per nanoparticle is not accurately quantified [22], it may not be possible to determine the proportion of the administered nanoparticle dose that has associated to the cells. Therefore, it is not straightforward to say whether dosage depletion limits nanoparticle association, or whether the plateau can be attributed to a carrying capacity. While we see a difference in the width of the dosage distribution between the two cases, it is unclear whether this would be observable when the dosage distribution is confounded by experimental measurement noise and biological heterogeneity. As such, it is critical to follow experimental protocols that allow for quantification of the relevant experimental measurements, and hence allow for reliable estimation of the biological parameters that dictate nanoparticle internalisation [40, 42, 43].

4. Discussion and conclusions

Nanoparticles are a promising avenue for the targeted delivery of therapeutics to specific cell types [1, 2, 3]. While this technology has seen recent success in specific areas [1], significant gaps remain in the understanding of nanoparticle-cell interactions. This hinders the effective development of nanoparticle-based therapeutics [2, 3, 4, 5]. One factor that complicates analysis and interpretation of standard experiments is heterogeneity in experimental data [6, 7, 8, 9, 10]. It is not straightforward to determine whether this heterogeneity arises from the underlying cell population, or from the stochastic nature of nanoparticle motion and nanoparticle-cell interactions [6, 7]. It is critical to identify whether significant biological heterogeneity is present, as it may imply the existence of a subpopulation of cells that do not respond to a particular treatment [13, 14]. Mathematical models have been employed to investigates the sources of heterogeneity previously [6, 7, 8, 9]; however, such investigations have relied on simplified models of nanoparticle-cell interactions, and neglect the potential impact of a range of biological processes.

Here we present a mathematical modelling framework that provides predictions of the level of heterogeneity expected to manifest in nanoparticle dosage due to the presence of specific biological mechanisms. As such, if we know that particular biological mechanisms are relevant, we are able to identify how much heterogeneity in dosage is unavoidable due to the stochastic nature of the nanoparticle internalisation process. Any additional heterogeneity can therefore be attributed to either experimental measurement error, which is well-established for techniques such as flow cytometry [44], or to heterogeneity in the underlying cell population [6, 7]. We include and investigate a range of biological mechanisms that are relevant for standard nanoparticle-cell experiments, including multistage nanoparticle internalisation, cell division, asymmetric nanoparticle inheritance and saturation of nanoparticle internalisation. We provide analytic expressions for the expected dosage distributions under certain simplifying assumptions. We demonstrate that in the presence of cell proliferation, the overall dosage distribution can be accurately approximated via a series of mixture distributions for the

cell subpopulations that have experienced a specific number of cell divisions. These mixture distributions allow for the mechanism behind the plateau in nanoparticle association to be identified, as there is a distinction between the mixture distributions arising from cell division compared to those arising from dosage depletion, even though the overall dosage distributions are similar. A summary of the key results for each biological mechanism investigated, and whether analytic results can be obtained in each case, is presented in Table 1. The analytic results provide an efficient method for determining the expected nanoparticle dosage distribution.

Biological heterogeneity can be explicitly included in the model by allowing the rate parameters of biological processes to follow specified distributions [6, 7]. However, we leave this extension for future work, noting that the analytic results provide an efficient method for analysing the confounding effects of biological heterogeneity and heterogeneity arising from the stochastic nature of nanoparticle-cell interactions. While we have examined a broad suite of biological mechanisms, it would be instructive to further develop the mathematical model to incorporate other potentially relevant phenomena such as sedimentary nanoparticle transport [27], nanoparticle exocytosis (recycling), transyctosis and degradation [9], and cell death. Here, we have primarily focused on theoretical analyses of the model. However, there is significant potential for interfacing the model with experimental data to draw conclusions about the sources of heterogeneity present. Such investigations will provide quantitative estimates of biological parameters in the case where the experimental data is sufficient to parameterise the appropriate model. Moreover, in the case where the data is not sufficient, we can employ the model to guide experimental protocol with respect to the type and frequency of data that is required to be collected.

Code availability

All code to perform the model simulations is available on GitHub at https://github.com/celia2dow/Nanobio_Research_Project.

Acknowledgements

The authors would like to acknowledge the generous guidance, mentoring and support provided by the late Prof. Edmund Crampin. Edmund taught us to think deeply about biological problems, with a rigour informed by his background in physics. He is terribly missed, and we hope to honour his legacy by continuing to apply his lessons to help unravel new problems.

Funding

S.T.J. is supported by the Australian Research Council (Project No. DE200100988). M.F. is supported by a gift from the estate of Réjane Louise Langlois. This work was supported by the Australian National Health and Medical Research Council (NHMRC; Program Grant No. GNT1149990), the Australian Centre for HIV and Hepatitis Virology Research (ACH^2) .

Appendix A. Experimental details

We aimed to assess the internalisation of 100 nm nanoparticles by Jurkat T cells. We hypothesised that targeting the nanoparticles to different surface receptors would alter the uptake kinetics by triggering receptor-mediated endocytosis. To test this, we used a model nanoparticle system made of iron oxide coated with protein G, which is straightforward to functionalise with a targeting antibody. The targeting antibody was fluorescently labelled (AF647), which has the additional benefit of labelling the nanoparticles. Cells and nanoparticles were incubated for 1, 2, 4, 8, 24 and 48 hours, after which any nanoparticles remaining on the cell surface (external) were stained by incubating the cells with a secondary antibody (PE) that detects the primary targeting antibody. The fluorescence signal was measured via flow cytometry and processed via an arcsinh transform. No gating was performed.

References

[1] X. Hou, T. Zaks, R. Langer, Y. Dong, Lipid nanoparticles for mRNA delivery, Nature Reviews Materials 6 (12) (2021) 1078–1094.

[2] M. J. Mitchell, M. M. Billingsley, R. M. Haley, M. E. Wechsler, N. A. Peppas, R. Langer, Engineering precision nanoparticles for drug delivery, Nature Reviews Drug Discovery 20 (2) (2021) 101–124.

[3] S. Wilhelm, A. J. Tavares, Q. Dai, S. Ohta, J. Audet, H. F. Dvorak, W. C. Chan, Analysis of nanoparticle delivery to tumours, Nature Reviews Materials 1 (5) (2016) 1–12.

[4] S. Zhang, H. Gao, G. Bao, Physical principles of nanoparticle cellular endocytosis, ACS Nano 9 (9) (2015) 8655–8671.

[5] D. Sun, S. Zhou, W. Gao, What went wrong with anticancer nanomedicine design and how to make it right, ACS Nano 14 (10) (2020) 12281–12290.

[6] S. T. Johnston, M. Faria, E. J. Crampin, Isolating the sources of heterogeneity in nano-engineered particle–cell interactions, Journal of the Royal Society Interface 17 (166) (2020) 20200221.

[7] P. Rees, J. W. Wills, M. R. Brown, C. M. Barnes, H. D. Summers, The origin of heterogeneous nanoparticle uptake by cells, Nature Communications 10 (1) (2019) 1–8.

[8] H. D. Summers, P. Rees, M. D. Holton, M. Rowan Brown, S. C. Chappell, P. J. Smith, R. J. Errington, Statistical analysis of nanoparticle dosing in a dynamic cellular system, Nature Nanotechnology 6 (3) (2011) 170–174.

[9] H. D. Summers, C. P. Gomes, A. Varela-Moreira, A. P. Spencer, M. Gomez-Lazaro, A. P. Pêgo, P. Rees, Data-driven modeling of the cellular pharmacokinetics of degradable chitosan-based nanoparticles, Nanomaterials 11 (10) (2021) 2606.

[10] T. Turnbull, B. Thierry, I. Kempson, A quantitative study of intercellular heterogeneity in gold nanoparticle uptake across multiple cell lines, Analytical and Bioanalytical Chemistry 411 (28) (2019) 7529–7538.

[11] M. J. Ware, B. Godin, N. Singh, R. Majithia, S. Shamsudeen, R. E. Serda, K. E. Meissner, P. Rees, H. D. Summers, Analysis of the influence of cell heterogeneity on nanoparticle dose response, ACS Nano 8 (7) (2014) 6693–6700.

[12] B. Ouyang, W. Poon, Y.-N. Zhang, Z. P. Lin, B. R. Kingston, A. J. Tavares, Y. Zhang, J. Chen, M. S. Valic, A. M. Syed, P. MacMillan, J. Couture-Senécal, G. Zheng, W. C. W. Chan, The dose threshold for nanoparticle tumour delivery, Nature Materials 19 (12) (2020) 1362–1371.

[13] S. J. Altschuler, L. F. Wu, Cellular heterogeneity: do differences make a difference?, Cell 141 (4) (2010) 559–563.

[14] M. Greaves, C. C. Maley, Clonal evolution in cancer, Nature 481 (7381) (2012) 306–313.

[15] L. I. FitzGerald, A. P. Johnston, It's what's on the inside that counts: techniques for investigating the uptake and recycling of nanoparticles and proteins in cells, Journal of Colloid and Interface Science 587 (2021) 64–78.

[16] A. P. Johnston, Life under the microscope: quantifying live cell interactions to improve nanoscale drug delivery, ACS Sensors 2 (1) (2017) 4–9.

[17] N. D. Donahue, H. Acar, S. Wilhelm, Concepts of nanoparticle cellular uptake, intracellular trafficking, and kinetics in nanomedicine, Advanced Drug Delivery Reviews 143 (2019) 68–96.

[18] S. T. Johnston, M. Faria, E. J. Crampin, Understanding nano-engineered particle–cell interactions: biological insights from mathematical models, Nanoscale Advances 3 (8) (2021) 2139–2156.

[19] M. Faria, K. F. Noi, Q. Dai, M. Björnmalm, S. T. Johnston, K. Kempe, F. Caruso, E. J. Crampin, Revisiting cell–particle association in vitro: A quantitative method to compare particle performance, Journal of Controlled Release 307 (2019) 355–367.

[20] T. Lijster, C. Åberg, Asymmetry of nanoparticle inheritance upon cell division: effect on the coefficient of variation, PLOS ONE 15 (11) (2020) e0242547.

[21] H. D. Summers, M. R. Brown, M. D. Holton, J. A. Tonkin, N. Hondow, A. P. Brown, R. Brydson, P. Rees, Quantification of nanoparticle dose and vesicular inheritance in proliferating cells, ACS nano 7 (7) (2013) 6129–6137.

[22] C. Gottstein, G. Wu, B. J. Wong, J. A. Zasadzinski, Precise quantification of nanoparticle internalization, ACS Nano 7 (6) (2013) 4933–4945.

[23] J. A. Kim, C. Åberg, A. Salvati, K. A. Dawson, Role of cell cycle on the cellular uptake and dilution of nanoparticles in a cell population, Nature Nanotechnology 7 (1) (2012) 62–68.

[24] S. T. Johnston, M. Faria, E. J. Crampin, An analytical approach for quantifying the influence of nanoparticle polydispersity on cellular delivered dose, Journal of The Royal Society Interface 15 (144) (2018) 20180364.

[25] J. Cohen, G. DeLoid, G. Pyrgiotakis, P. Demokritou, Interactions of engineered nanomaterials in physiological media and implications for *in vitro* dosimetry, Nanotoxicology 7 (4) (2013) 417–431.

[26] P. M. Hinderliter, K. R. Minard, G. Orr, W. B. Chrisler, B. D. Thrall, J. G. Pounds, J. G. Teeguarden, ISDD: A computational model of particle sedimentation, diffusion and target cell dosimetry for *in vitro* toxicity studies, Particle and Fibre Toxicology 7 (1) (2010) 1–20.

[27] J. Cui, M. Faria, M. Björnmalm, Y. Ju, T. Suma, S. T. Gunawan, J. J. Richardson, H. Heidari, S. Bals, E. J. Crampin, F. Caruso, A framework to account for sedimentation and diffusion in particle–cell interactions, Langmuir 32 (47) (2016) 12394–12402.

[28] S. T. Johnston, M. J. Simpson, R. E. Baker, Modelling the movement of interacting cell populations: a moment dynamics approach, Journal of Theoretical Biology 370 (2015) 81–92.

[29] M. J. Simpson, K. A. Landman, B. D. Hughes, Multi-species simple exclusion processes, Physica A: Statistical Mechanics and its Applications 388 (4) (2009) 399–406.

[30] S. T. Johnston, M. J. Simpson, D. L. S. McElwain, How much information can be obtained from tracking the position of the leading edge in a scratch assay?, Journal of the Royal Society Interface 11 (97) (2014) 20140325.

[31] M. J. Simpson, K. A. Landman, B. D. Hughes, Cell invasion with proliferation mechanisms motivated by time-lapse data, Physica A: Statistical Mechanics and its Applications 389 (18) (2010) 3779–3790.

[32] C. A. Yates, M. J. Ford, R. L. Mort, A multi-stage representation of cell proliferation as a markov process, Bulletin of Mathematical Biology 79 (12) (2017) 2905–2928.

[33] C. Åberg, J. A. Kim, A. Salvati, K. A. Dawson, Reply to 'The interface of nanoparticles with proliferating mammalian cells', Nature Nanotechnology 12 (7) (2017) 600–603.

[34] E. Panet, T. Mashriki, R. Lahmi, A. Jacob, E. Ozer, M. Vecsler, I. Lazar, A. Tzur, The interface of nanoparticles with proliferating mammalian cells, Nature Nanotechnology 12 (7) (2017) 598–600.

[35] A. Noel, D. Makrakis, Algorithm for mesoscopic advection–diffusion, IEEE Transactions on Nanobioscience 17 (4) (2018) 543–554.

[36] C. Wilhelm, F. Gazeau, J. Roger, J. Pons, J.-C. Bacri, Interaction of anionic superparamagnetic nanoparticles with cells: kinetic analyses of membrane adsorption and subsequent internalization, Langmuir 18 (21) (2002) 8148–8155.

[37] D. T. Gillespie, Approximate accelerated stochastic simulation of chemically reacting systems, The Journal of Chemical Physics 115 (4) (2001) 1716–1733.

[38] J. E. Gentle, Computational Statistics, Springer, 2019.

[39] G. P. Yanev, Exponential and hypoexponential distributions: some characterizations, Mathematics 8 (12) (2020) 2207.

[40] M. Faria, S. T. Johnston, A. J. Mitchell, E. J. Crampin, F. Caruso, Bio-nano science: Better metrics would accelerate progress, Chemistry of Materials 33 (19) (2021) 7613–7619.

[41] R. Chartrand, Numerical differentiation of noisy, nonsmooth data, International Scholarly Research Notices (2011).

[42] M. Faria, M. Björnmalm, K. J. Thurecht, S. J. Kent, R. G. Parton, M. Kavallaris, A. P. Johnston, J. J. Gooding, S. R. Corrie, B. J. Boyd, P. Thordarson, A. K. Whittaker, M. M. Stevens, C. A. Prestidge, C. J. H. Porter, W. J. Parak, T. P. Davis, E. J. Crampin, F. Caruso, Minimum information reporting in bio–nano experimental literature, Nature Nanotechnology 13 (9) (2018) 777–785.

[43] H. S. Leong, K. S. Butler, C. J. Brinker, M. Azzawi, S. Conlan, C. Dufès, A. Owen, S. Rannard, C. Scott, C. Chen, et al., On the issue of transparency and reproducibility in nanomedicine, Nature Nanotechnology 14 (7) (2019) 629–635.

[44] L. Wang, R. A. Hoffman, Standardization, calibration, and control in flow cytometry, Current Protocols in Cytometry 79 (1) (2017) 1–3.